NASA Contractor Report 172206

HOMOGENEOUS NUCLEATION AND DROPLET GROWTH IN NITROGEN

Edward H. Dotson

GEORGE WASHINGTON UNIVERSITY
Joint Institute for Advancement of Flight Sciences
Hampton, Virginia 23665

Cooperative Agreement NCC1-44
September 1983

National Aeronautics and
Space Administration

Langley Research Center
Hampton, Virginia 23665

TABLE OF CONTENTS

Page

LIST OF TABLES

LIST OF FIGURES

LIST OF SYMBOLS

a	sound speed, m/sec
A	nozzle area, m^2
A_d	droplet surface area, m^2
A^*	nozzle throat area, m^2
c	airfoil chord length, m
c_p	specific heat at constant pressure, J/kg-K
c_v	specific heat at constant volume, J/kg-K
C_p	pressure coefficient, defined eq. 1
d	rigid sphere diameter, m
g	mass fraction of condensate
h	specific enthalpy, J/kg
$h^*_{T_o}$	reference specific enthalpy, J/kg
h'	Planck's constant, J-sec
I	moment of inertia, kg m^2
J	nucleation rate, droplets/m^3-sec
k	Boltzman's constant, J/k
Kn	Knudsen number, defined eq. 40
L	latent heat, J/kg
$\bar{\ell}$	mean free path, m
m	mass of one molelcule, kg
M	Mach number
$M_{L\text{-max}}$	maximum local Mach number
$\dot{m}$	mass flow rate, kg/sec
n	molecules per droplet
N_A	Avogadro's number, molecules/moles

p	pressure, N/m^2 or atm (1 atm = 101325 N/m^2)
p_o	reference pressure, N/m^2
Pr	Prandtl number, defined eq. (63)
q	dynamic pressure, N/m^2
Q_{rep}	Lothe and Pound replacement factor
r	droplet radius, m
R	specific gas constant, 296.81 J/kg-K
R_c	Reynolds number based on chord
s	specific enthalphy, J/kg-K
$s^*_{T_o}$	reference value of specific entropy
t	time, sec
T	temperature, K
T_o	reference temperature, K
u	velocity, m/sec
v	specific volume, m^3/kg
W	net work in forming droplet, J
x	distance from leading edge, m
α	angle of attack, deg
γ	ratio of specific heats, c_p/c_v
δ	Tolman constant, m
$\Delta h_{\ell g}$	change in enthalpy from gas to liquid, J/kg
η	viscosity, N-sec/m^2
λ	thermal conductivity J/m-K-sec
μ	molecular weight, kg/mole
ξ	thermal accommodation coefficient
π	ratio of circle circumference to diameter, 3.14159
ρ	density, kg/m^3

ρ_c'	equivalent condensate density, kg/m^3
ρ_T	total density of the flow, kg/m^3
σ	surface tension, N/m
σ_∞	planar surface tension, N/m
ϕ	correction factor to nucleation rate

Subscripts

c	condensate
CL	classical
ℓ	liquid
LP	Lothe and Pound
NI	nonisothermal
r	droplet
RK	Reiss or Kikuchi
s	solid
sat	saturation
t	total conditions
∞	freestream conditions
( )	no subscript denotes gas properties

Superscripts

*	critical
o	zero pressure conditions

HOMOGENEOUS NUCLEATION AND DROPLET GROWTH IN NITROGEN

INTRODUCTION

Transonic cryogenic wind tunnels, such as the Langley 0.3-Meter Transonic Cryogenic Tunnel (TCT) and the National Transonic Facility (NTF), are designed to increase Reynolds number, R_c, by lowering the temperature of the nitrogen test gas to cryogenic temperatures. Figure 1 shows that for nitrogen there is a significant increase in Reynolds number when going to the lower temperatures. Onset of condensation due to either heterogeneous (pre-existing seed particles) or homogeneous (the gas forms its own seed particles) nucleation limits the minimum operating temperature and, consequently, the maximum Reynolds number capability.[1] This minimum operating temperature can be conservatively limited to temperatures corresponding to saturation at the maximum local Mach number, M_{L-max}, over the airfoil. (Saturation occurs when the pressure and temperature of the gas are on the vapor-pressure curve.) However, as reported in reference 1, for the 0.3-m TCT, heterogeneous nucleation has only been detected below temperatures corresponding to freestream saturation. Therefore, if condensation effects occur over an airfoil in the 0.3-m TCT at temperatures above freestream saturation, it is probably due to homogeneous nucleation. Because of an energy barrier to the onset of homogeneous nucleation, however, onset will not take place until tunnel temperatures are below those corresponding to saturation at M_{L-max}.

As shown for the example in figure 1, if condensation effects do not occur until the temperature is reduced to that value corresponding to free-stream saturation, the Reynolds number can be increased by 25

percent over the Reynolds number at the temperature for saturation at $M_{L\text{-}max}$. In the present work, a computer model of the homogeneous nucleation process and growth of nitrogen condensate for flows over airfoils is developed to predict the onset of homogeneous nucleation and thus to be able to take advantage of as much of the Reynolds number capability of cryogenic tunnels as possible.

This computer model is restricted to the supersonic region over the airfoil because this is where condensation due to homogeneous nucleation will occur first and also because of difficulties in making calculations through sonic conditions. In order to further simplify the calculations, a one-dimensional analysis is used rather than a more complicated two-dimensional analysis. With regard to the applicability of the one-dimensional model, Wagner[2] determined that the differences between one- and two-dimensional calculations for his condensation calculations are smaller than the differences between condensed and uncondensed flow. Wagner, therefore, concluded that the one-dimensional simulation should account for the main condensation effects in a qualitatively correct manner. Therefore, it is assumed herein that a one-dimensional calculation is adequate in predicting condensation effects over a two-dimensional airfoil.

Using a two-step procedure, the condensation over the supersonic section of an airfoil is predicted by first calculating the geometry of an equivalent one-dimensional nozzle from the condensation-free, isentropic pressure distributions measured over the airfoil, as shown in figure 2. The nondimensional pressure coefficient, C_p, is given by

$$C_p = \frac{p - p_\infty}{q_\infty}, \qquad (1)$$

and $\frac{A}{A^*}$ is the nondimensional area of the one-dimensional nozzle with A* being the throat area at sonic speeds. By following an approach similar to earlier one-dimensional models of flow through a supersonic nozzle, as described in references 3, 4, and 5, the second step solves for condensation in the equivalent nozzle. In the present study, this step involves integrating the continuity, energy, and momentum equations along with a condensation equation based on the classical liquid droplet theory (CLDT) of homogeneous nucleation and Gyarmathy's droplet growth equation, using a fourth order Runge-Kutta integration scheme. Also incorporated into this program is the Beattie-Bridgeman,[6] equation of state which can be reduced to the ideal gas equation of state, if desired, and a variety of suggested corrections to the CLDT - Tolman,[7] nonisothermal,[8] Lothe and Pound,[9] and that due to either Reiss[10] or Kikuchi.[11]

Data from airfoil experiments in the Langley 0.3-m TCT and from earlier nozzle experiments are used to evaluate the various corrections to the CLDT, the real gas effects, and the sensitivity of the model to certain parameters.

EQUATIONS

Flow Equations

Since the flow over the supersonic section of an airfoil can be approximated by the flow through an equivalent nozzle, the condensing flow can be described following an approach similar to earlier models in references 3, 4, and 12. For this study, the flow is assumed to be one-dimensional, steady, frictionless at the boundary and adiabatic--no heat transfer across the boundary. Instead of assuming an ideal gas as in earlier models, nitrogen is assumed to be a real gas which obeys the Beattie-Bridgeman[6] equation of state. The condensing droplets are assumed to occupy negligible volume with respect to the remaining vapor and have the same speed as surrounding gas.

Continuity

Since the flow is steady through the nozzle and the droplets are assumed to be at the same speed as the flow, the continuity equation can be written as

$$\rho_T \, uA = \dot{m} = \text{constant} \tag{2}$$

The total density, ρ_T, is made up of two parts, such that

$$\rho_T = \rho_c' + \rho \tag{3}$$

where ρ_c' is the equivalent density of the condensate dispersed throughout the same volume as the vapor density ρ. By solving for ρ, equation (3) can be expressed as

$$\rho_T\left(1 - \frac{\rho_c'}{\rho_T}\right) = \rho \tag{4}$$

Since ρ_c' and ρ_T are over the same volume, ρ_c'/ρ_T can be replaced by the mass fraction of the condensate, g, which is defined as the ratio of the condensate mass to the total mass. Therefore, the total density ρ_T can be expressed as

$$\rho_T = \frac{\rho}{1-g} \tag{5}$$

By substituting equation (5) into equation (2), the continuity equation can be expressed as

$$\frac{\rho}{1-g} uA = \dot{m} \tag{6}$$

The differential form of the continuity equation is then written as

$$\frac{1}{\rho}\frac{d\rho}{dx} + \frac{1}{1-g}\frac{dg}{dx} \quad \frac{1}{u}\frac{du}{dx} + \frac{1}{A}\frac{dA}{dx} = 0 \tag{7}$$

Momentum

From the assumptions that the droplets move at the same speed as the gas, and that the flow is frictionless at the boundary of the nozzle, the momentum equation takes the form

$$\rho_T\, u \frac{du}{dx} = -\frac{dp}{dx}$$

or

$$\frac{\rho}{1-g} u \frac{du}{dx} = -\frac{dp}{dx} \tag{8}$$

Energy

From the assumptions of no heat transfer across the nozzle boundary and steady one-dimensional flow, the energy equation can be obtained from the first law of thermodynamics as

$$\frac{u^2}{2} + h - g\,[c_p\,(T - T_r) + L(T_r)] = \text{const} \tag{9}$$

Because the first term in the brackets and the difference between latent heat evaluated at T and T_r are small compared to the rest of the equation, the energy equation can be simplified to the following form which is also used in references 2, 3, 4, and 12:

$$\frac{u^2}{2} + h - gL = \text{const} \tag{10}$$

where L is calculated at the gas static temperature. The differential form of the energy equation is then written as

$$u\,\frac{du}{dx} + \frac{dh}{dx} - g\,\frac{dL}{dx} - L\,\frac{dg}{dx} = 0 \tag{11}$$

Equation of state

To complete the solution of equations (7), (8), and (11), the equation of state is added to the flow equations. Because pressure is a function of density and temperature, the derivative can be expressed as

$$\frac{dp}{dx} = \left(\frac{\partial p}{\partial \rho}\right)_T \frac{d\rho}{dx} + \left(\frac{\partial p}{\partial T}\right)_\rho \frac{dT}{dx} \tag{12}$$

The derivative of specific enthalpy of the gas, h, can be expressed as

$$\frac{dh}{dx} = c_p \frac{dT}{dx} + \left(v - T\left(\frac{\partial v}{\partial T}\right)_p\right) \frac{dp}{dx} \tag{13}$$

from reference 13. By substituting $\frac{1}{\rho}$ for v and using the mathematical identity

$$\left(\frac{\partial p}{\partial \rho}\right)_T \left(\frac{\partial \rho}{\partial T}\right)_p \left(\frac{\partial T}{\partial p}\right)_\rho = -1 \tag{14}$$

equation (14) can be written as

$$\frac{dh}{dx} = c_p \frac{dT}{dx} + \left(\frac{1}{\rho} - \frac{T}{\rho^2}\left(\frac{\partial p}{\partial T}\right)_\rho \Big/ \left(\frac{\partial p}{\partial \rho}\right)_T\right) \frac{dp}{dx} \tag{15}$$

Solution of flow equations

Because $\frac{dg}{dx}$ can be calculated from the nucleation and growth rate equations, to be discussed later, and A is already determined, these values are treated as known quantities. Therefore, the linear system of equations (7), (8), (11), (12), and (15) remain for the derivatives $\frac{dp}{dx}$, $\frac{d\rho}{dx}$, $\frac{dT}{dx}$, $\frac{du}{dx}$, and $\frac{dh}{dx}$. Because the latent heat, L, is primarily a function of temperature, the derivative may be expressed as

$$\frac{dL}{dx} = \frac{dL}{dT} \frac{dT}{dx} \tag{16}$$

By substituting equations (8), (15), and (16) into equation (11) and collecting terms, the energy equation can then be written as

$$u\frac{du}{dx}\left(1 - \frac{1}{1-g} + \frac{T}{\rho(1-g)}\left(\frac{\partial p}{\partial T}\right)_\rho \Big/ \left(\frac{\partial p}{\partial \rho}\right)_T\right) + \frac{dT}{dx}\left(c_p - g\frac{dL}{dT}\right) = L\frac{dg}{dx} \tag{17}$$

which can be expressed in the form

$$C_1 \, u \frac{du}{dx} + C_2 \frac{dT}{dx} = C_3 \tag{18}$$

By solving equation (12) for $\frac{d\rho}{dx}$, substituting this result along with equation (8) into (7), and collecting terms, the continuity equation can be written as

$$u\frac{du}{dx}\left[-\frac{1}{(1-g)(\partial p/\partial \rho)_T} + \frac{1}{u^2}\right] + \frac{dT}{dx}\left[-\frac{1}{\rho}\frac{(\partial p/\partial T)_\rho}{(\partial p/\partial \rho)_T}\right] = -\frac{1}{1-g}\frac{dg}{dx} - \frac{1}{A}\frac{dA}{dx} \tag{19}$$

which can be expressed in the form

$$E_1 \, u \frac{du}{dx} + E_2 \frac{dT}{dx} = E_3 \tag{20}$$

Using Kramer's Rule, equations (18) and (20) can be solved simultaneously for $\frac{du}{dx}$ and $\frac{dT}{dx}$ in the following form

$$\frac{du}{dx} = \frac{1}{u} \cdot \frac{C_3 E_2 - C_2 E_3}{C_1 E_2 - C_2 E_1} \tag{21}$$

$$\frac{dT}{dx} = \frac{C_1 E_3 - C_3 E_1}{C_1 E_2 - C_2 E_1} \tag{22}$$

From the continuity equation (7), $\frac{d\rho}{dx}$ is determined as

$$\frac{d\rho}{dx} = -\rho \left(\frac{1}{1-g}\frac{dg}{dx} + \frac{1}{u}\frac{du}{dx} + \frac{1}{A}\frac{dA}{dx}\right) \tag{23}$$

Finally, $\frac{dp}{dx}$ is calculated from the momentum equation as

$$\frac{dp}{dx} = -\frac{\rho}{1-g} u \frac{du}{dx} \tag{8}$$

Hence, from equations (8), (21), (22), (23), and $\frac{dg}{dx}$ calculated from the nucleation and growth rate equations to be discussed in the next section, the condensing flow over the airfoil can be solved.

Homogeneous Nucleation

The condensation over an airfoil is assumed to be the result of droplets formed by the homogeneous nucleation of the nitrogen gas although the following equations are for any pure vapor. In the homogeneous nucleation process there is a size-dependent energy barrier which must be overcome such that all droplets with radius, r, less than some critical droplet radius, r*, will tend to evaporate while all droplets with radius larger than r* will be stable and grow. The critical radius is calculated from the Gibbs-Thomson[3] or Kelvin[14] equation

$$\ln\left(\frac{p}{p_{sat}}\right) = \frac{2\sigma}{\rho_\ell R T r^*}$$

with the result that

$$r^* = \frac{2\sigma}{\rho_\ell R T \ln\left(p/p_{sat}\right)} \tag{24}$$

where σ is the surface tension of the droplet, ρ_ℓ is the droplet density, and p_{sat} is the saturated vapor pressure calculated at the temperature of the gas, T. At saturation $p/p_{sat} = 1$ and $r^* = \infty$; however, r* decreases as p/p_{sat} increases and the probability

increases that random collisions of gas molecules will result in a growing droplet with radius larger than r^*.

The formation rate of critical-sized droplets is represented by the classical liquid droplet theory, CLDT, which assumes that spherical, liquid droplets are formed which retain the bulk liquid properties and are in thermal equilibrium with the surrounding vapor. For real-gas behavior, the vapor molecular density is expressed as $\frac{\rho}{m}$ rather than as the ideal gas value of $\frac{p}{kT}$. Therefore, the present author modified the pre-exponential term in the nucleation equation found in Wu[3] so that the CLDT can be expressed as

$$J_{CL} = \frac{\rho^2}{\rho_\ell} \left(\frac{2\sigma}{\pi m^3}\right)^{1/2} \exp\left(-\frac{W}{kT}\right) \tag{25}$$

where m is the mass of one molecule and

$$W = \frac{4}{3} \pi r^{*2} \sigma \tag{26}$$

is the net work[12] required for the formation of the critical-sized droplet. This net work is the energy barrier which must be overcome to form a droplet. In terms of the critical droplet surface area, A_d, equation (26) can be rewritten as

$$W = A_d \sigma/3 \tag{27}$$

As mentioned in reference 12, this result is also true for the formation of a solid cluster of molecules, or crystal of quite general shape where σ is a "surface tension"-like term based on the free surface

energy of the crystal in contact with a vapor. Some assumptions must be made concerning the shape of the crystal.[12] For lack of another equation, the CLDT (eq. (25)) is used in references 3, 4, 5, and 15 to determine the formation rate of crystals where the surface tension σ has been replaced by the free surface energy of the solid.

Substituting equation (24) into (25) gives the following expression:

$$J_{CL} = \frac{\rho^2}{\rho_\ell} \left(\frac{2\sigma}{\pi m^3}\right)^{1/2} \exp\left(-\frac{16\pi\sigma^3}{3kT\,(\rho_\ell\, kT\, \ell n(p/p_{sat}))^2}\right) \qquad (28)$$

Because of the dependence of the dominant exponential term on the inverse of $\ell n^2\ p/p_{sat}$, homogeneous nucleation does not occur until the flow is supersaturated ($p/p_{sat} > 1$). The exponential term is also proportional to σ^3; therefore, the nucleation rate is very sensitive to errors in the surface tension. For conditions appropriate for transonic, cryogenic wind tunnels, a ten-percent error in σ could result in a nucleation rate change of 10^6 and an error of 3K in total temperature at which onset of condensation is predicted to occur.

Modifications to Homogeneous Nucleation

Since the introduction of CLDT, many researchers have attempted to improve the theory by accounting for some of the physics that are disregarded by the basic CLDT. This section reviews some of the best-known efforts to improve the nucleation rate predicted by the classical theory.

Tolman

Because of possible error in assuming the planar value for surface tension of a liquid droplet, the effect of droplet size on surface tension has been studied by several people.[16] One of the first to study the effect of droplet size on surface tension was Tolman[7] who developed a correction to surface tension of the form

$$\sigma = \sigma_\infty/(1 + \frac{2\delta}{r^*}) \tag{29}$$

where σ_∞ is the planar surface tension and δ is a constant based on the intermolecular distances of the liquid which is on the order of 10^{-10}m for several fluids.[7] Tolman comments that less and less confidence can be placed in this expression as droplets get smaller and smaller.[7] Typical droplets for the present calculations contained 50 molecules. Applying Tolman's correction to the surface tension, Sivier[5] calculated the critical radius in equation (29) to be

$$r^* = r^* (\sigma_\infty) - 2\delta \tag{30}$$

where $r^*(\sigma_\infty)$ is calculated from equation (24) using σ_∞. Therefore, by using equation (29) and (30) and the appropriate Tolman constant, δ, the surface tension can be corrected and thus the CLDT can be modified.

Lothe and Pound

Because they felt that the free energy of formation in the CLDT, represented by the net work in equation (26), was not complete, Lothe and Pound[9] proposed a correction to the CLDT which includes the free

translational and rotational energies. Using the macroscopic or planar surface tension, σ_∞, the Lothe and Pound correction factor can be written in the following form from reference 3:

$$J = \phi_{LP} \cdot J_{CL} \tag{31}$$

where

$$\phi_{LP} = \frac{\left[\left(\frac{2\pi n^* m_c k T}{h^2}\right)^{3/2} \frac{k T}{p}\right] \left[\left(\frac{8\pi^2 I^* kT}{h^2}\right)^{3/2} \sqrt{\pi}\right]}{Q_{rep}} \tag{32}$$

where

$$n^* = \frac{4}{3} \pi r^{*3} \rho_c / m_c \tag{33}$$

and the moment of inertia, I^*, of critical spherical droplets is given by

$$I^* = \frac{2}{5} n^* m_c r^{*2} \tag{34}$$

The replacement factor, Q_{rep}, which compensates for the six degrees of freedom introduced from the translational and rotational energies, is based on the free energies of separation. For water, Q_{rep} has been approximated between 10^4 and 10^8 in reference 17. With $Q_{rep} = 10^4$, ϕ_{LP} has been estimated at 10^{16}.[17] Because of the added translational and rotational energies, the Kelvin equation should be modified to include the correction term[14]

$$\ln (p/p_{sat}) = \frac{2 \sigma}{\rho_c R T r^*} - \frac{4}{n^*} \tag{35}$$

which increases the nucleation rate by an additional factor of 10-100 for the present calculations.

Reiss or Kikuchi

Reiss[10] agrees with Lothe and Pound[9] that the CLDT should be corrected, but he suggests that the Lothe and Pound correction is only appropriate in connection with crystalline particles. In an early work, Reiss and Katz[18] developed an expression similar to that of Lothe and Pound, but concluded that, for a liquid, the free rotational energy is already contained in the bulk description of the free energy of formation. Kikuchi[19] extended the work of Reiss, et.al.[20] and also concluded that no rotational effects should be included for a liquid droplet. In the appendum of Reiss,[10] Reiss compares his and Kikuchi's[11] correction and concludes them to be essentially the same except that Kikuchi takes droplet curvature dependence into account. Disregarding curvature dependence, this correction will be labelled ϕ_{RK} for either Reiss or Kikuchi and can be written as

$$\phi_{RK} = \frac{v}{v_\ell} = \frac{\rho_\ell}{\rho} \tag{36}$$

so that the nucleation rate can be expressed as

$$J = \phi_{RK} J_{CL} \tag{37}$$

Nonisothermal

In contradiction to the assumption that the forming droplets are in thermal equilibrium with the condensing vapor which, as discussed by

Wu[3], is valid only when a large quantity of carrier gas is present to dissipate the heat of condensation, Wu, following Feder, et.al,[8] incorporated a correction factor to account for the temperature differences between the droplets and the vapor that result from the necessary heat transfer between the forming droplets and the surrounding gas. When simplified for a pure vapor, this nonisothermal correction factor[3] can be written as

$$\phi_{NI} = \frac{\gamma + 1}{\gamma+1 + 2(\gamma - 1)\left[\frac{L}{RT} - \frac{1}{2} - \left(1 - \frac{T}{\sigma}\frac{\partial\sigma}{\partial T}\right) \ln (p/p_{sat})\right]^2} \tag{38}$$

so that the nucleation rate can be expressed as

$$J = \phi_{NI} \cdot J_{CL} \tag{39}$$

This nonisothermal multiplier reduces the nucleation rate by factors as large as 22 for the conditions analyzed herein. With regard to the growth equation proposed by Gyarmathy[21] discussed in the next section, a nonisothermal correction factor would not be proper because he assumes that the droplets and vapor are in thermal equilibrium at critical conditions.

Gyarmathy Droplet Growth Equation

A parameter known as Knudsen number, Kn, is used to define different regimes of droplet growth and is given as[22]

$$Kn = \frac{\bar{\ell}}{2r} \tag{40}$$

where $\bar{\ell}$ is the mean free path of a gas molecule and r is the droplet radius. For free-molecular flow, $Kn \gg 1$, and for continuum flow, $Kn \ll 1$. Most of the earlier programs in references 3, 4, and 5 used a free molecular growth equation, but because of the relatively high gas densities which exist in transonic cryogenic tunnels, a growth equation that describes droplet growth in free-molecular, transition and continuum regimes is needed.[22] As described in reference 22, Gyarmathy developed a continuum equation which closely approximates droplet growth in the free-molecular regime as well. For a pure vapor, Gyarmathy's equation takes the form of

$$\frac{dr}{dt} = \frac{\lambda}{\rho_\ell \Delta h_{\ell g}} \cdot \frac{1}{1 + \left(\frac{2\sqrt{8\pi}}{1.5 Pr \xi} \frac{\gamma}{(\gamma+1)}\right) Kn} \cdot \frac{T_r - T}{r} \tag{41}$$

where P_r is the Prandtl number of the gas, ξ is the thermal accommodation coefficient, which is assumed to be 1, and T_r is the temperature at the surface of the droplet expressed as[21]

$$T_r = T + (T_{sat} - T)\left(1 - \frac{r^*}{r}\right) \tag{42}$$

where T_{sat} is the saturation temperature calculated at the pressure of the gas. The change in enthalpy, $\Delta h_{\ell g}$, from the gas at T to the

liquid at T_r is expressed as

$$\Delta h_{\ell g} = c_p(T - T_r) + L\ (T_r). \tag{43}$$

By neglecting $c_p(T - T_r)$ and evaluating the latent heat L at the temperature of the gas rather than T_r in the energy equation (9) and in equation (43), the total temperature of condensation onset is typically reduced by less than 0.25K. Therefore, by approximating $\Delta h_{\ell g}$ as $L(T)$, equation (41) can be rewritten as

$$\frac{dr}{dt} = \frac{\lambda}{\rho_\ell L} \cdot \frac{1}{1 + \left(\frac{2\sqrt{8\pi}}{1.5\ Pr\ \xi}\ \frac{\gamma}{\gamma+1}\right) Kn} \cdot \frac{T_r - T}{r} \tag{44}$$

This droplet growth equation assumes no coagulation of droplets. When droplet radius is close to r^*, the droplet growth rate is slow because $T_r \approx T$. Evaporation of droplets is approximated by equation (44).

Calculation of Condensate

The condensate formed in the two-phase flow is determined from the integral of the condensate mass fraction $g(x)$[3], which is written as

$$g(x) = \frac{1}{\dot{m}} \int_{-\infty}^{x} \frac{4\pi}{3} \rho_c\ J(\delta) A(\delta)\ r^3\ (\delta, x)\ d\delta \tag{45}$$

where g, the nucleation rate J, and the effective nozzle area A are functions of position along the nozzle, x. The quantity $r(\delta,x)$ is the radius at x of a droplet formed at δ, which can be written as

$$r(\delta, x) = r(\delta, \delta) + \int_{\delta}^{x} \frac{\partial\, r(\delta, \epsilon)}{\delta\, \epsilon}\, d\, \epsilon \qquad (46)$$

where $r(\delta, \delta)$ is the critical radius at δ and where

$$\frac{\partial r}{\partial \delta} = \frac{1}{u(\delta)} \frac{dr}{dt} \qquad (47)$$

where $\frac{dr}{dt}$ is determined from equation (44). Differentiation of equation (45) with respect to x gives

$$\frac{dg}{dx} = \frac{1}{\dot{m}} \left(\frac{4\pi}{3} \rho_c\, J(x)\, A(x)\, r^3(x,x) + \int_{-\infty}^{x} 4\pi \rho_c\, J(\delta)\, A(\delta)\, r^2(\delta,x) \frac{1}{u(x)} \frac{dr}{dt}\, d\delta\right) \qquad (48)$$

where $\frac{\partial r}{\partial x}$ is replaced by $\frac{1}{u(x)} \frac{dr}{dt}$ from equation (47). Equation (48) shows that the increase in mass fraction consists of the droplet mass fraction being created in dx and of the growth of particles created before the current x location.

Using a fourth order Runge-Kutta integration scheme, equations (48), (47), (21), (22), (23), and (8) are solved for the flow variables g, r, u, T, ρ, and p. The properties of gaseous and condensed nitrogen which are necessary in solving these flow equations are discussed in the next section.

PROPERTIES OF NITROGEN

The properties of gaseous, liquid, and solid nitrogen are needed in predicting the formation of liquid or solid nitrogen droplets from nitrogen vapor.

Gas Properties

The properties of gaseous nitrogen are known relatively well down to the triple point (temperature, 63.148K, and pressure, .1237 atm, at which solid, liquid, and gaseous states of nitrogen coexist).[23] The extrapolated equations for the nitrogen gas properties can only be assumed to be valid for describing the nitrogen gas below the triple point and the metastable gas which exists in the liquid regime before the gas condenses.

Equation of state

The Beattie-Bridgeman (B-B) equation of state for nitrogen is used herein to introduce real gas effects. This equation of state is surprisingly accurate and is represented by[6]

$$p = \rho RT\left(1 - \frac{c}{T^3}\rho\right)\left[1 + B_0\,\rho(1 - b\rho)\right] - A_0\rho^2(1 - a\rho) \qquad (49)$$

where the values of the constants for nitrogen are listed in table 1. By setting these constants to zero, the ideal gas equation of state is obtained

$$p = \rho RT \qquad (50)$$

Using the B-B or ideal gas equation of state, the following expressions are used for calculating the specific enthalpy, h, specific entropy, s, heat capacities, c_v and c_p, and sound speed,

a, for nitrogen gas:[6]

$$h = h^*_{T_o} + \int_{T_o}^{T} \rho\left[\frac{p}{\rho^2} - \frac{T}{\rho^2}\left(\frac{\partial p}{\partial T}\right)_\rho\right]d\rho + \frac{p - \rho RT}{\rho} + \int_{T_o}^{T} c_p^o \, dT \qquad (51)$$

$$s = s^*_{T_o} + \int_{T_o}^{T} \frac{c_p^o}{T} dT - R \ln\left(\frac{\rho RT}{p_o}\right) + \int_{o}^{\rho} \left[\frac{R}{\rho} - \frac{1}{\rho^2}\left(\frac{\partial p}{\partial T}\right)_\rho\right]d\rho \qquad (52)$$

$$c_v = c_v^o - T\int_o^\rho \frac{T}{\rho^2}\left(\frac{\partial^2 p}{\partial T^2}\right)_\rho d\rho \qquad (53)$$

$$c_p = c_v + T\left(\frac{\partial p}{\partial T}\right)_\rho^2 / \left[\rho^2\left(\frac{\partial p}{\partial \rho}\right)_T\right] \qquad (54)$$

$$a = \left[\frac{c_p}{c_v}\left(\frac{\partial p}{\partial \rho}\right)_T\right]^{1/2} \qquad (55)$$

where $h^*_{T_o}$ = 309500 J/kg and $s^*_{T_o}$ = 6836.09 J/kg-k are reference values of specific enthalpy and entropy, the reference pressure, p_o, is 101325 N/m^2, and the reference temperature, T_o, is 298.15K.[24] The zero pressure values of specific heats, c_p^o and c_v^o are represented by the following ideal expressions

$$c_p^o = \frac{\gamma}{\gamma - 1} R \qquad (56)$$

where the ratio of specific heats, $\gamma = \frac{c_p}{c_v}$, for "ideal" nitrogen or any ideal diatamic gas, is 1.4. Therefore

$$c_p^o = 3.5R \qquad (56a)$$

and

$$c_v^o = c_p^o - R \qquad (57)$$

In figure 3, the results of calculating c_p using the B-B equation of state (eq. (50)) are compared with the constant ideal gas value. Although not shown, similar results would be calculated for c_v and γ. As in the following figure the gas properties are calculated along the vapor pressure, V-P, curve (saturation boundary) and constant pressure lines of 0.1 and 2 atms. The constant pressure lines, which are the range of local static pressures typically encountered during airfoil tests, extend from the gas regime across the V-P curve and into the metastable gas regime by about 15K, which would be below the temperatures at which the onset of condensation was observed during the airfoil experiments to be discussed in a later section.

Mean free path

The mean free path, $\bar{\ell}$, is the average distance traveled by a molecule between collisions. The ideal expression assuming a rigid spherical molelcule[25],[26] is used for $\bar{\ell}$ as shown

$$\bar{\ell} = \frac{1}{\sqrt{2}\,\pi\,\frac{\rho}{m}\,d^2} \tag{58}$$

where $\frac{\rho}{m}$ is the molecular volume and d is the rigid sphere diameter. By substituting $d = 3.75 \times 10^{-10}$m for nitrogen,[26] the mean free path for gaseous nitrogen can be written as

$$\bar{\ell} = \frac{7.44 \times 10^{-8}}{\rho} \tag{59}$$

Thermal conductivity

The thermal conductivity of nitrogen, λ, can be calculated using equation from Jacobsen[23] which is made up of two terms

$$\lambda = \lambda_0(T) + \Delta \lambda_E(\rho) \tag{60}$$

where the dilute gas contribution, λ_0, and the excess, or dense, fluid contribution, $\Delta\lambda_E$, which is basically a function of density only, are listed in table 2.

In Jacobsen,[23] there is an additional term which is the enhancement due to the influence of the critical point. For the present study, this term is deleted because it is generally small and because the high pressures (~ 30 atms) in the neighborhood of the critical point are not typical of condensation onset in transonic cryogenic wind tunnels. Equation (60) is compared over the temperature range of interest with a Sutherland-type expression used by Wagner[2] which is given as

$$\lambda = 2.067 \times 10^{-3} \frac{\sqrt{T}}{1 + 111/T} \tag{61}$$

As shown in figure 4, the results of both equations are similar but the λ calculated with equation (60) is slightly pressure dependent. For the present studies, the Sutherland-type expression is used.

Viscosity

The viscosity, η, of nitrogen is calculated from an equation in Jacobsen,[23] which contains two terms and is written as

$$\eta = \eta_0(T) + \Delta \eta_E(\rho) \qquad (62)$$

where the dilute gas contribution, η_0, and the excess, or dense, fluid contribution, η_E, which is primarily dependent on density, are listed in table 3. In Jacobsen,[23] there is another expression for $\Delta\eta_E$ for when the gas density ρ is greater than 800 kg/m^3, but this term is not included because gas densities of this magnitude are not typical of condensation onset in transonic cryogenic wind tunnels. Equation (62) is compared over the temperature range of interest with a Sutherland-type expression used by Wagner,[3] which is given as

$$\eta = 1.378 \times 10^{-6} \frac{\sqrt{T}}{1 + 103/T} \qquad (63)$$

For the range of local pressures during the airfoil tests, the results of both equations are similar for the temperatures above 70 K as shown in figure 5, but the η calculated from equation (62) is slightly pressure dependent. At the lower temperatures, the results of equation (62) are questionable and, in fact, the Sutherland-type expression for viscosity is recommended in place of the Jacobsen expression.

Prandtl number

The Prandtl number, Pr, is defined as

$$Pr = \frac{c_p \eta}{\lambda} \qquad (64)$$

For constant pressures and the Jacobsen expression for thermal conductivity, λ (eq. (60)), and viscosity, η (eq. (62)), and the

ideal value of $c_p = 3.5R$, the Prandtl number approaches 0.73 for temperatures above 70K. This value agrees with the constant value for Pr of 0.72 (see fig. 6a) calculated using the Sutherland-type expressions for λ (eq. (61)) and η (eq. (63)) from Wagner[2] and assuming the ideal value for c_p of 3.5R. However, at the lower temperatures, Pr increases significantly from the Sutherland value of 0.72, because of the increase in Jacobsen's expression for viscosity at the lower temperatures (see fig. 5).

Using the B-B equation of state and thus the real-gas value of c_p, the Prandtl numbers calculated using the Jacobsen and Sutherland expressions for λ and η are in good agreement with each other at temperatures above 70K, where both calculations are greater than the ideal gas value of Pr (see figs. 6b and 6c) because of the real gas value of c_p which is shown in figure 3. Even though, at the lower temperatures, the real gas values of c_p approach the ideal gas c_p of 3.5R, the Prandtl numbers calculated from the Jacobsen and Sutherland-type expressions for λ and η again do not agree because of the low-temperature differences in η (see fig. 6b and 6c). The Prandtl number calculated from the Sutherland-type equations for λ and η might be appropriate for both above and below the triple point because of (1) the good agreement between the Jacobsen and Sutherland-type expressions for η above 70K and λ over the full temperature range for constant pressures and (2) the more reasonable η values calculated from Sutherland-type expression at temperatures below 70K although there is no direct experimental evidence at temperatures below the triple point.

Condensate Properties

The properties of solid and liquid nitrogen are needed in predicting condensation. The liquid properties of nitrogen are known relatively well from the critical point[23] (33.555 atm, 126.20 K) down to the triple point. For the metastable flow expansions below the triple point, there is some uncertainty as to whether or not the formation of liquid condensate continues or the formation of solid condensate begins. Unfortunately, there appear to have been no studies done on this possibly abrupt phase change for the properties of the condensing metastable nitrogen. For β-phase solid nitrogen, which exists between the triple point down to approximately 35.5 K[27], a vapor pressure curve and density equation are derived from existing data and used along with theoretical expressions for the latent heat of sublimation and surface tension because no appropriate data exist. As mentioned before, the droplets are assumed to have the same properties as the bulk condensate, with the exception of surface tension which is sometimes modified using Tolman's corrections (eqs. (29) and (30)).

Vapor-pressure curve

The vapor pressure, V-P, curve (fig. 7) represents the saturation line between gas and liquid or gas and solid. A more complicated expression for the V-P curve between the critical and triple point found in Jacobsen[23] is approximated very well by a simpler expression found in Dodge and Davis, [28] which is of the form

$$p_{sat} = 10^{(a - b/T)} \cdot c \tag{65}$$

where the constants are listed in table 4.

For β -phase solid nitrogen, the V-P curve is represented by a similar expression from Frels, Smith, and Ashworth[29] where the values for the constants are also listed in table 4. The expressions used for the V-P curve of nitrogen in the earlier programs[3],[4],[5] are similar to these expressions but with slight variations in the constants.

Density of condensate

The liquid nitrogen density is well known and is evaluated by a curve fit to data in Jacobsen.[23] The curve fit shown in figure 8 is

$$\rho_\ell = 28.0134\ (34.65+.01381\ T_\ell - .001145\ T_\ell^2) \qquad (66)$$

The expressions for liquid nitrogen density used in earlier programs give similar results; for example, from Sivier[5]

$$\rho_\ell = 1181 - 4.8\ T_\ell \qquad (67)$$

However, the value of 808.4 kg/m^3 used by Düker and Koppenwallner[15] is considered the best value if the temperature dependence is disregarded.

The β -phase solid nitrogen density is evaluated by this author with a curve fit to data in Scott,[27] although his data point for the density at T = 44 K has been excluded. The resulting curve fit is

$$\rho_s = 1068.49 - 1.97830\ T_s \qquad (68)$$

Griffin[4] and Sivier[5] extrapolated their expressions for liquid density below the triple point in order to estimate the solid nitrogen density; however, this extrapolation could lead to serious errors in

density as shown in figure 8. Düker and Koppenwallner[15] and Wu[3] used a value of 1026 kg/m^3 which appears to overestimate the solid nitrogen density for the temperature range of interest.

Latent heat

The latent heat of vaporization, which is the heat necessary to convert a liquid to at a given temperature a given mass of liquid to the same mass of vapor, is calculated from a curve fit to the difference of enthalpies between gaseous and liquid nitrogen in Jacobsen.[23] This curve fit can be written as follows:

$$L = 2326.3\ (147.283 - 1.6851\ T + .01974\ T^2 - .00010716\ T^3) \quad (69)$$

For β -phase solid nitrogen, no appropriate data exist for the latent heat of sublimation, which is the heat necessary to convert at a given temperature a given mass of solid to the same mass of vapor. Consequently, a theoretical expression is calculated from the Clausius-Clapeyron equation:

$$\frac{d\ p_{sat}}{dT} = \frac{L}{T(v - v_s)} \quad (70)$$

where $\frac{d\ p_{sat}}{dT}$ is the slope of the V-P curve and v is the specific volume of the gas. The slope of the V-P curve is determined from the derivative of equation (65) with respect to T, which can be expressed as follows:

$$\frac{d\ p_{sat}}{dT} = \ln (10)\ \frac{b}{T^2}\ p_{sat} \quad (71)$$

By equating equations (70) and (71), solving for L, and replacing v with $\frac{1}{\rho}$, the latent heat of sublimation can be expressed as

$$L = \frac{b\, p_{sat}}{T} \left(\frac{1}{\rho} - \frac{1}{\rho_s}\right) \ln 10 \qquad (72)$$

where p_{sat} and b are from reference 29. As can be seen in figure 9, a relatively constant value of 2.43×10^5 J/kg for the nitrogen latent heat of sublimation is calculated from equation (72) for both ideal and real gas equation for ρ. This value agrees well with Wu's[3] value of 2.42×10^5 J/kg for the nitrogen latent heat of sublimation. Griffin[4] and Sivier [5] extended the latent heat of vaporization below the triple point. Extension of equation (69), the curve fit to Jacobsen's values of latent heat for the liquid, below the triple point in figure 9 shows that a markedly different value of nitrogen latent heat of sublimation could result. Therefore, the current program uses a constant value of 2.43×10^5 J/kg for the nitrogen latent heat of sublimation.

Surface tension

Surface tension is a familiar concept for liquids and can be readily measured. For liquid nitrogen, the surface tension can be expressed as[23]

$$\sigma = 0.0297074 \left(1 - T_\ell / 126.2\right)^{1.27135} \qquad (73)$$

while earlier expressions such as the one by Sivier[5]

$$\sigma = .02394 - .0001933\, T_\ell \qquad (74)$$

give similar results, as shown in figure 10. However, for solids, a comparable, physical surface tension is not normally thought of or measured. Nevertheless, there is a common link between liquids and solids; namely that both have an associated surface energy. For purposes of CLDT, surface tension can be viewed as surface energy divided by area. In a very useful theoretical work, Tabor[30] outlined an approach which relates the latent heat of sublimation with the free surface energy of a solid. Tabor's expression is

$$\sigma = 0.267 \left(\frac{L_s \mu}{N_A}\right) \left(\frac{N_A \rho_s}{\mu}\right)^{2/3} \qquad (75)$$

where 0.267 is a factor appropriate for the [100] face of a face-centered cubic (fcc) solid. For other faces and structures, the numerical factor should be changed by a small amount.[30] A reasonable average value for the numerical factor is 0.3.[30] This relation should best apply to van der Waals solids such as solid neon, argon, and krypton.[30] However, experimental verifications for these solids do not exist. Solid nitrogen is also a van der Waals solid. For the comparisions with data in Tabor,[30] equation (75) generally overpredicts the surface energies for several solids; therefore, an expression of this type is considered to be the upper limit of free surface energy of a solid.

Since the structure of β-phase solid nitrogen is hexagonal close packed, (hcp), the present author modified Tabor's expression (see Appendix A). Assuming that the droplets form along the lowest energy surface which is the [0001] face of a hcp solid, the result of the modification to equation (75) is

$$\sigma = .229 \frac{L_s \mu}{N_A} \left(\frac{N_A}{\mu} \rho_s\right)^{2/3} \tag{76}$$

where the constant is smaller than the value of .267 estimated by Tabor. Because the latent heat of sublimation is 2.43×10^5 J/kg, equation (76) can be simplified to the following expression

$$\sigma = 2.00 \times 10^{-4} (\rho_s)^{2/3} \tag{77}$$

where ρ_s is calculated from equation (68).

In figure 10, the free surface energy or surface tension calculated from equation (77) is within 10 percent of Düker and Koppenwallner's[15] empirically determined value of 0.0185 N/m. Wu[3] set the surface tension of solid nitrogen at 0.0124 N/m which is significantly lower than the values calculated from equation (77). Griffin[4] and Sivier[5] extrapolated their respective expressions for the liquid nitrogen surface tension below the triple point, which results in very different values for surface tension. As mentioned in the section discussing the CLDT, CLDT can be particularly sensitive to surface tension and so these differences can be very important.

In fact, by examining equation (28), it can be seen that the ratio of σ^3/ρ_ℓ^2 is an important quantity to predicting the nucleation rate. Consequently, knowing the values of the surface tension and density used in a particular paper is necessary to properly compare the different theoretical expressions different researchers have used for predicting the onset of homogeneous nucleation. In other words, many differences in theoretical expressions may be overshadowed by variations in

σ^3/ρ_s^2 from one paper to another. For example, in figure 11, the ratio of σ^3/ρ_s^2 calculated from ρ_s (eq. (68)) and σ (modified Tabor theory eq.(77)) is $8.00 \times 10^{-12} \frac{N^3 m^3}{kg^2}$ which is 33 percent greater than the ratio value of $6.01 \times 10^{-12} \frac{N^3 m^3}{kg^2}$ calculated from Düker and Koppenwallner's[15] expressions for ρ_s and σ. If Düker and Koppenwallner's value of solid nitrogen surface tension is combined with the density calculated from equation (68), the resulting modified ratio would be 8- to 19-percent greater than their original value. Also included in figure 11 are the values of σ^3/ρ_s^2 calculated from Wu's[3] and Sivier's[5] expressions for σ and ρ_s.

RESULTS AND DISCUSSION

Comparisons between theoretical predictions and experimental data are next used to evaluate the performance of CLDT and the various corrections to CLDT, the sensititity of the calculations to certain parameters, and the sensitivities of the nucleation expressions to the slight differences in pressure and temperature that arise when the expansion isentrope is calculated using the more precise Beattie-Bridgeman equation of state for nitrogen instead of the approximate ideal equation of state for an ideal diatomic gas. The data for these comparisons will be from experiments in the Langley 0.3-m TCT using the 0.152 m DFVLR-constructed CAST-10 airfoil and from earlier nozzle experiments by Dankert[31] and Nagamatsu and Willmarth[32].

CAST-10 Airfoil

The 0.152m DFVLR CAST-10 airfoil was tested in the Langley 0.3-m TCT in order to observe possible condensation effects due to homogeneous nucleation in the supersonic flow region over an airfoil. The freestream Mach number was held constant at 0.65 and the angle of attack, α, was set at 6 degrees. With these conditions, the maximum local Mach number, M_{L-max}, over the airfoil was approximately 1.4 for the total pressure range tested.

Comparison of the CAST-10 airfoil data with the one-dimensional computer model discussed in the previous sections is restricted to the supersonic region over the airfoil, because this is where condensation due to homogeneous nucleation will occur first (see fig. 12) and because of difficulties in mathematically calculating through the sonic condition. Furthermore, the experimental scatter in the condensation-free data near the recompression shock is large while the scatter in the

data in the supersonic region is small, which again suggests comparisons in the supersonic region. Because the computer model cannot calculate through a sonic condition, the calculations must start at an x/c location of 0.007, where the flow is already past M = 1. Because only small deviations in pressure and, hence, area distribution are to be studied, the one-dimensional model should be a good approximation. Assuming an ideal gas equation of state, the classical liquid droplet theory, CLDT, (eq. 25), along with several modifications, are compared with the experimental condensation data. These modifications include classical theory as modified by Tolman with $\delta = 0.25 \times 10^{-10}$ m in equations 29 and 30, labelled CLDT-T; classical theory as modified by Lothe and Pound (eq. 31), labelled CLDT-LP; classical theory as modified by Reiss or Kikuchi (eqs. 37), labelled CLDT-RK.

Data for the CAST-10 test were taken during experiments whose total conditions are represented by the three lines in figure 13 identified as p_t = 5 atm, $R_c = 15 \times 10^6$ and $R_c = 34 \times 10^6$. The total temperatures were lowered along either a constant value of total pressure or along paths of varying total pressure total temperature which provided constant values of R_c. The upper temperature limits of the experiments were chosen so that no effects due to condensation could occur in the supersonic region and the minimum temperatures were chosen to be below those corresponding to freestream saturation.

The two higher pressure cases (the 5 atm and the 34×10^6 R_c lines) displayed the onset of condensation effects due to the formation of liquid nitrogen because the total temperatures remained above 88K which is the total temperature at which the local temperature at $M_{L\text{-max}} = 1.4$ is 63.148K, the triple point temperature. These two total

temperatures at which onset occurred for the higher pressure cases are 14K below the total temperature at which saturation occurs for M_{L-max} = 1.4 at the same total pressure as at onset. However, they are above the total temperature for which freestream saturation occurs.

The lower pressure case (15 million R_c) displayed no condensation effects even down below freestream saturation. If condensation had occurred, solid nitrogen would have been formed because the total temperature was below 88K. The predictions of the computer models are compared wth the CAST-10 airfoil data for liquid nitrogen condensation in the next section.

Liquid nitrogen

As mentioned, for the 34×10^6 R_c and 5 atm CAST-10 experiments, the condensed phase is liquid nitrogen. The data showing the liquid nitrogen condensation effects on the local pressure for the 34×10^6 R_c experiment are shown in figure 14 as the pressure coefficient deviation, $\Delta C_p = C_p - C_{p,\text{no cond.}}$, plotted against the x/c location over the airfoil. For p_t = 3.7 atm and T_t = 96K, the CAST-10 data exhibit little or no condensation effects. However, at p_t = 3.6 atm and T_t = 94K, the CAST-10 data show definite condensation effects on pressure. Using the unmodified CLDT, the computer model underpredicts condensation effects at 94K (the prediction did not rise above the zero line). Use of $\delta = 0.25 \times 10^{-10}$m (a value of δ arbitrarily chosen) in CLDT-T results in good agreement with the CAST-10 data at T_t = 94K. The computer model with CLDT-RK gives the same order of magnitude of condensation effects as the CAST-10 data at T_t = 94K. Use of CLDT-LP with $Q_{rep} = 10^3$, which is the largest proposed value of Q_{rep} according to reference 17, and which would result in the smallest value

of nucleation, greatly overpredicts condensation effects at 94K as well as 96K where no effects are shown experimentally. This poor prediction is consistent with the statement in an earlier section, namely, that the Lothe and Pound correction may only be appropriate to describe the formation of solid particles. The nonisothermal correction is not shown because it reduces the CLDT prediction even further. Therefore, the predicted condensation effects are less than with the CLDT.

The rapid formation of condensation effects shown in figure 14 is due to the reduction of total temperature and pressure which is characteristic of homogeneous nucleation. The sensitivity of condensation effects to small T_t changes is shown in figure 15 where results for the CLDT-RK condensation model for 94.0K and 93.7K are compared. The 0.3K reduction in T_t, which is well within the experimental error of 0.5K at these conditions, results in a doubling of the ΔC_p and brings the results into better agreement with the CAST-10 data at 94.0K. (Reducing T_t by 0.3K typically doubles the predicted ΔC_p for CLDT and the other corrections as well.) Thus, it is difficult to tell whether using CLDT-RK is more accurate than CLDT-T because of the uncertainty in the measured temperatures.

In figure 16, comparisons of various theoretical predictions are made with the 5 atm CAST-10 data. At T_t = 101K, there are possible condensation effects, but effects are uncertain because the experimental error in ΔC_p is of the same magnitude as the deviations observed. At 99K, the computer model with CLDT underpredicts condensation effects on pressure, but with either CLDT-T ($\delta = 0.25 \times 10^{-10}$m) or CLDT-RK it gives the same order of magnitude deviations as the data before significant condensation growth occurs. If a smaller value of δ is used with

CLDT-T, better agreement would result, t this would then lead to poorer agreement in figure 14. This discrepancy at x/c greater than 0.15 could be due to limitations of using the one-dimensional model in describing the two-dimensional flow over the airfoil. Use of CLDT-LP is not shown because it is not appropriate for the homogeneous nucleation of liquid nitrogen droplets. The nonisothermal correction lowers the predicted condensation effects below the CLDT line and is again not shown.

The pressure distribution from the 5 atm CAST-10 airfoil experiment is now used to examine the predicted condensation onset of liquid nitrogen for each modification to the CLDT. Also, the sensitivity of CLDT to a 10-percent reduction in surface tension and to utilization of the B-B equation of state to describe the pressures and temperatures along the expansion isentrope rather than the less accurate ideal equation of state are examined. In table 5, p_t is held constant at 5 atm and T_t is varied in each version of the computer model until the ΔC_p at $x/c = 0.25$ matches the baseline value of $\Delta C_p = 0.0266$, which is calculated using CLDT at $T_t = 99K$. The ratio J/J_{CL} is the increase in the nucleation rate over the CLDT where both are calculated for the new T_t at $M_{L-max} = 1.4$. As seen in table 5, the unmodified CLDT can predict the condensation onset T_t of nitrogen flow over the CAST-10 airfoil within 2K of the T_t assuming CLDT-T or CLDT-RK is correct. Use of the CLDT-LP, which is not expected to apply above the triple point for nitrogen, with $Q_{rep} = 10^8$ increases the condensation onset T_t by 4.8K. A 10-percent reduction in surface tension could result in a 3K increase in condensation onset T_t and a 10^6 increase in the nucleation rate at $M_{L-max} = 1.4$; therefore, the calculations are

very sensitive to the surface tension. Using the B-B equation of state (eq. 50) with the CLDT shows that the real gas behavior of the expanding gas results in smaller differences in onset T_t than those found when using the CLDT-T or CLDT-RK in the computer model. For further predictions of the liquid nitrogen condensation onset T_t, CLDT-RK will be used in the computer model because (1) it agrees within the experimental error of the data, and (2) the Tolman constant, δ, in the CLDT-T is arbitrary and does not do a better job than CLDT-RK when both figures 14 and 16 are considered. In the next section, the appropriate correction to the CLDT for the formation of solid nitrogen is studied by comparing with the $R_c = 15 \times 10^6$ CAST-10 airfoil data.

Solid Nitrogen

Formation of solid nitrogen is assumed to occur when local temperature during the condensation process is below the triple point temperature of nitrogen. Because of the uncertainty in the values of density and surface tension, the various expressions discussed in the section on nitrogen properties are evaluated by comparison between the $R_c = 15 \times 10^6$ CAST-10 airfoil data and the computer model. The surface tension and density are calculated from equations 77 and 68, respectively, while the CLDT, CLDT-T, or CLDT-LP are used in the the computer model. CLDT-RK is not used for describing the solid nitrogen formation because it was derived for liquid formation. Additional versions to be examined are CLDT with Düker and Koppenwallner's expressions for σ and ρ_s, labelled CLDT-DK; CLDT-T with Sivier's expressions for σ, ρ_s, and $\delta = 0.325 \times 10^{-10}$m, labelled CLDT-SIV; and CLDT with Wu's expressions for σ and ρ_s, labelled CLDT-WU.

The CAST-10 airfoil experiment in which solid nitrogen condensation could have been formed is the $R_c = 15x10^6$ experiment. But, as shown in figure 17, no measurable condensation effects were found down to p_t = 1.3 atm and T_t = 83K which are below the total conditions for freestream saturation at $M_\infty = 0.65$. Similarly, using CLDT, CLDT-T with $\delta = 0.25x10^{-10}$m , CLDT-LP with $Q_{rep} = 10^4$ (this value of Q_{rep} is the smallest of the range given in ref. 17 and would lead to the largest predicted value of nucleation rate), or CLDT-DK, the computer model predicted no condensation effects on the measure static pressure. However, as shown in figure 17, condensation effects are greatly overpredicted using CLDT-SIV or CLDT-WU. Therefore, from these data, the conclusion can be drawn that the expressions of Wu and Sivier for solid nitrogen density and surface tension are not appropriate for the prediction of solid nitrogen condensation for these conditions. Further analysis of solid nitrogen formation is covered in the next section by studying nozzle data.

Nozzles

Because of the limited CAST-10 airfoil data below the triple point temperature of nitrogen, previous nozzle experiments by Dankert[31] and Nagamatsu and Willmarth[32] are studied in order to evaluate possible corrections to the CLDT in this regime. Nozzle area is calculated from the isentropic or no-condensation pressure distribution where the pressure coefficients are calculated by using the dynamic pressure at an arbitrary Mach number. The first comparison will be made to the data of Dankert published in reference 31.

Dankert

The most useful data of Dankert[31] for the present comparisons are his free-jet nozzle data from his figure 34 in which p_t = 3.0 atm and the throat diameter is 0.005m. For T_t = 125K, 160K, and 175K, the computer model dramatically underpredicts condensation effects using CLDT, CLDT-T, or CLDT-DK which are not shown in figure 18. In figure 19, the computer model using CLDT-LP with $Q_{rep} = 10^4$ agrees well with data for T_t = 125K and reasonably well with data for T_t = 160 K and 175K before a significant amount of condensation occurs, which causes the assumptions used in the model to become invalid. In figure 18b, onset of condensation effects are overpredicted for all three cases using CLDT-WU except when large amounts of condensate are present, where the assumptions used in the model are inaccurate. In the next section, further comparisons are made with wedge nozzle data.

Nagamatsu and Willmarth

Because Sivier's computer model in reference 5 agrees with the wedge nozzle data from figure 14 of Nagamatsu and Willmarth[32] for run 9-5 with p_t = 8.21 atm and T_t = 295K, the present computer model is compared with these data. No condensation effects are predicted using CLDT, CLDT-T, CLDT-LP, CLDT-DK, or CLDT-SIV. Condensation effects are also underpredicted using CLDT-WU as shown in figure 19. This disagreement between the computer model and the Nagamatsu and Willmarth data could be due to either impurities in the nitrogen used by Nagamatsu and Wilmarth or in the assumptions in the computer model. In particular, since Sivier's properties for the solid nitrogen density and surface tension are used in CLDT-SIV, the primary difference between Sivier's model and CLDT-SIV developed herein is that Sivier assumes the droplets

are at saturation temperature regardless of size. The present model uses a radius-dependent droplet temperature based on reference 21, which assumes the critical-sized droplets are at the gas static temperature. Sivier's assumption results in a larger nucleation rate and, thus, an increase in condensation effects, which results in agreement for the Nagamatsu and Willmarth data, but it also would result in dramatic overprediction for the $R_c = 15x10^6$ CAST-10 data and in the Dankert data.

The present computer model using CLDT-LP with $Q_{rep} = 10^4$ will be used to predict the onset of solid nitrogen condensation over the CAST-10 airfoil in the next section because (1) it agrees with the Dankert data[46] and (2) does not overpredict condensation effects for the $R_c = 15x10^6$ CAST-10 airfoil experiment.

Predicted Onset of Homogeneous Nucleation

The total conditions at which onset of condensatin due to the homogeneous nucleation will occur over the 0.152m DFVLR CAST-10 airfoil at $M_\infty = 0.65$ and $\alpha = 6^0$ can be predicted using the present computer model. Homogeneous nucleation is represented by the CLDT-RK for liquid nitrogen and the CLDT-LP with $Q_{rep} = 10^4$ for solid nitrogen, although more experimental comparison data are needed to verify these choices. Growth of the droplets is represented by Gyarmathy's[21] radius-dependent droplet growth equation. In figure 20, the predicted onset of condensation effects is said to occur when the pressure deviates from the no-condensation pressure by 0.25 percent at $x/c = 0.25$. This is an arbitrary location ahead of the recompression shock for the CAST-10 experiment, which is the pressure distribution used in predicting this onset curve. For other pressure distributions, a different location may be appropriate, depending on the shock location. The predicted onset of

liquid nitrogen condensation agrees well with the experimental onset which was measured from the CAST-10 data. Below p_t = 3 atm, exact prediction of homogeneous nucleation may be unimportant for the 0.152m CAST-10 airfoil because the predicted onset of condensation falls below freestream saturation, where condensation on pre-existing seed particles (heterogeneous nucleation) can occur upstream of the airfoil and influence the aerodynamic data at temperatures above which homogeneous nucleation could occur. The inflection of the predicted onset curve at p_t = 2.5 atm is due to part of the flow being above and part of the flow being below the triple point during the calculation.

CONCLUDING REMARKS

A computer model of the homogeneous nucleation and growth of nitrogen condensate is developed for flows over airfoils which is capable of predicting the onset of condensation effects and, thus, the minimum operating temperatures without condensation effects for cryogenic wind tunnels. And from these temperatures, the maximum Reynolds number capability of a cryogenic wind tunnel can be predicted for a given configuration. For predicting liquid nitrogen condensation effects, the results of comparing the computer model and the experimental data for the 0.152m CAST-10 airfoil with $M_\infty = 0.65$ and $\alpha = 6^0$ are summarized as follows:

1. The computer model using the classical liquid droplet theory underpredicts condensation effects over the CAST-10 airfoil.
2. In order to get good agreement with the CAST-10 airfoil, the classical theory needs to be increased by a small factor such as the arbitrary Tolman constant of 0.25×10^{-10}, or the Reiss or Kikuchi correction.
3. Using the Lothe and Pound correction, condensation effects are greatly overpredicted for the case of liquid nitrogen condensation.
4. The nonisothermal correction to the classical theory further underpredicts condensation effects.
5. With the Beattie-Bridgeman equation of state used in calculating the expansion isentrope, the change in condensation effects is relatively small.
6. The calculations are very sensitive to the value of surface tension.

7. With the Reiss or Kikuchi correction to the classical theory, the computer model indicates that below p_t = 3 atm for the 0.152m CAST-10 airfoil with M_∞ = 0.65 and $\alpha = 6^0$, exact prediction of homogeneous nucleation of nitrogen may be unimportant because the predicted onset of condensation falls below freestream saturation, where heterogeneous nucleation can occur upstream of the airfoil and influence the aerodynamic data at temperatures above which homogeneous nucleation could occur.
8. To further validate the onset curve, more data need to be taken. These data must be taken very acurately because of the high sensitivity of the onset of condensation to total temperature.

In predicting the conditions which would give rise to effects due to the condensation of solid nitrogen, the results of comparing the computer model with experimental data are summarized in the following:

1. The surface tension and density are both important when comparing the nucleation rates of solid nitrogen because of the dependence of the nucleation equation on σ^3/ρ_c^2.
2. Using Wu's and Sivier's expressions for solid nitrogen surface tension and density, the classical theory dramatically overpredicts condensation effects for the CAST-10 airfoil data.
3. A theoretical expression for the surface tension of solid nitrogen is calculated from a modified version of Tabor's expression for surface tension.

4. Use of the classical theory with the Lothe and Pound correction $Q_{rep} = 10^4$, density from the Scott data and the expression for surface tension mentioned above, agrees with the Dankert free-jet data while use of the classical theory with Wu's surface tension and density overpredicts the onset of condensation effects.
5. Comparison of the present computer model with the Nagamatsu and Willmarth nozzle data and Sivier's computer model indicates that assuming droplet temperatures equal to satuation temperature rather than initially at gas temperature could greatly increase nucleation rate, although this assumption would be controversial.
6 Before any definitive conclusions can be made concerning onset of solid nitrogen formation, further studies on the properties of solid nitrogen and more experimental data are needed.

REFERENCES

1. Hall, Robert M.: Real Gas Effects II-Influence of Condensation on Minimum Operating Temperatures of Cryogenic Wind Tunnels. Cryogenic Wind Tunnels, AGARD-LS-111, May 1980, pp. 7-1 - 7-21.
2. Wagner, Bernhard: Estimation of Simulation Errors and Investigations on Operating Range Extensions for the European Transonic Wind Tunnel ETW. Dornier Report FB 81BF/8B, Dornier GmbH, March 1981.
3. Wu, Benjamin J. C.: Computer Programs for Calculating Condensation Rate in Steady, Adiabatic Expansions in Supersonic Nozzles. Dept. of Engineering and Applied Science, Yale University, 1974 (Available from DTIC as AD 775 257)
4. Griffin, James L.: Digital Computer Analysis of Condensation in Highly Expanded Flows. ARL 63-206, U. S. Air Force, November 1963.
5. Sivier, Kenneth R.: Digital Computer Studies of Condensation in Expanding One-Component Flows. ARL-65-234, U. S. Air Force, November 1965. (Available from DTIC as AD 628 543)
6. Hall, Robert M.: Real Gas Effects I - Simulation of Ideal Gas Flow by Cryogenic Nitrogen and Other Selected Gases. Cryogenic Wind Tunnels, AGARD-LS-111, May 1980, pp. 5-1 - 5-16.
7. Tolman, R. C.: The Effect of Droplet Size on Surface Tension. J. Chem. Phys., Vol. 17, No. 3, March 1979, pp. 333-337.
8. Feder, J.; Russell, K. C.; Lothe, J.; and Pound, G. M.: Homogeneous Nucleation and Growth of Droplets in Vapors. Adv. Phys. Vol 15, 1966, pp. 111-178.

9. Lothe, J.; and Pound, G. M.: Recommendations of Nucleation Theory. J. Chem. Phys., Vol. 36, No. 8, April 1962, pp. 2080-2085.

10. Reiss, H.: The Replacement Free Energy in Nucleation Theory. Advances in Colloid and Interface Sci., Vol. 7, Elsevier Sci. Pub. Co., Amsterdam, 1977, pp. 1-66.

11. Kikuchi, R.: Statistical Mechanics of a Liquid Droplet. Advances in Colloid and Interface Sci., Vol. 7, Elsevier Sci. Pub. Co., Amsterdam, 1977, pp. 67-102.

12. Wegener, Peter P.; and Mack, L. M.: Condensation in Supersonic and Hypersonic Wind Tunnels. Advances in Applied Mechanics, Vol. V., 1958, pp. 307-447.

13. Wark, Kenneth: Thermodynamics. Second Ed., McGraw-Hill Book Co., 1971.

14. Nishioka, K.; and Pound, G. M.: Homogeneous Nucleation in Vapor. Surface and Colloid Science, E. Matijevic, Ed., Vol. 8, Wiley-Interscience, New York, 1976, pp. 297-393.

15. Düker, M.; and Koppenwallner, G.: Comparisons Between Experimental Observations and Predictions Obtained with Classical Homogeneous Nucleation Theory for Nitrogen Condensation in Large Freejet Experiments. Presented as Paper 172 at 12th Intl. Symposium RGD, Charlottesville, VA, July 7-11, 1980.

16. Vogelsbeger, W.: Influence of Curvature-Dependent Surface Tension on the Free Energy of Formation of Microclusters. Chemical Physics Letters, Vol. 74, No. 1, August 1980, pp. 143-146.

APPENDIX

MODIFIED TABOR THEORY FOR SURFACE ENERGY OF SOLID NITROGEN

Tabor[30] outlined an approach which related the latent heat of sublimation to the free surface energy.[6] Basing his expression on the [100] face of a face-centered cubic (fcc) solid, he derived the following equation for surface energy

$$\sigma = .267 \left(\frac{L_s \mu}{N_A}\right) \left(\frac{N_A \rho_s}{\mu}\right)^{2/3} \qquad \text{A-1}$$

where the constant .267 changes by small amounts for other faces and structures.[30] Therefore, because β - phase solid nitrogen is a hexagonal closed-packed (hcp) solid, equation A-1 must be modified. Assuming that the droplets form along the lowest energy surface which is the [0001] face for a hcp solid, the surface energy is recalculated following the basic approach outlined in Tabor.[30]

On the [0001] face of a hcp solid, each surface molecule has 9 "nearest neighbors", whereas inside each crystal structure each molecule has 12 nearest neighbors. If each crystal contains a total of N atoms with N_s surface atoms, the total bond energy of the crystal, counting only nearest-neighbor interaction is

$$\frac{1}{2} \Delta\varepsilon \left[12(N-N_s) + 9\, N_s\right] = \frac{1}{2} \Delta\varepsilon \left[12N - 3N_s\right] \qquad \text{A-2}$$

where $\Delta\varepsilon$ is the potential energy between each molecule and its neighbor, and where the factor of $\frac{1}{2}$ is introduced to avoid counting each bond twice.

If there were no surface atoms, the energy would be $\frac{1}{2}\Delta\epsilon\ 12N$. Therefore, the energy is reduced by $\frac{3}{2}\Delta\epsilon\ N_s$. Because $\Delta\epsilon$ is negative, this is a positive increase in energy which can be associated with the surface energy. If the surface area of the crystal is A, the surface energy can be identified as

$$\sigma A = \frac{3}{2}\Delta\epsilon\ N_s \qquad \text{A-3}$$

Therefore, equation A-3 can be solved for σ

$$\sigma = \frac{3}{2}\Delta\epsilon\ \frac{N_s}{A} = \frac{3}{2}\Delta\epsilon\ z \qquad \text{A-4}$$

where z is the surface molecules per m^2.

The latent heat of sublimation can be expressed in terms of $\Delta\epsilon$ for a closed pack structure, such as a hcp structure, by the expression

$$L_s = \frac{1}{2} \cdot 12 \cdot \Delta\epsilon \cdot \frac{N_A}{\mu} \qquad \text{A-5}$$

or

$$L_s = 6 \cdot \Delta\epsilon \cdot \frac{N_A}{\mu}$$

(Note: In Tabor's method L is in J/mole, but for equation A-5, N_A is divided by the molecular weight, μ, because L has units of J/kg.) Equation A-5 can be solved for $\Delta\epsilon$ as

$$\Delta\epsilon = \frac{L_s\ \mu}{6\ N_A} \qquad \text{A-6}$$

and then $\Delta\varepsilon$ can be replaced in equation A-4 so that

$$\sigma = \frac{3}{2}\left(\frac{L_s\,\mu}{6\,N_A}\right) z = \frac{L_s\,\mu}{4\,N_A} z \qquad \text{A-7}$$

For a hcp lattice, the volume occupied by each molecule is $\frac{1}{\sqrt{2}} a^3$, where a is the distance between the center of one molecule and the center of its nearest neighbor. If μ is the molecular weight and ρ_s the density, the volume of each molecule is also represented by

$$\frac{\mu}{N_A\,\rho_s} = \frac{1}{\sqrt{2}} a^3 \text{ or } a^3 = \frac{\sqrt{2}\,\mu}{N_A\,\rho_s} \qquad \text{A-8}$$

For the [0001] face of a hcp solid, the area occupied by each molecule is $\frac{\sqrt{3}}{2} a^2$. The number of molecules per m^2, z, is $\frac{2}{\sqrt{3}\,a^2}$. Therefore, from A-8,

$$z = \frac{2}{\sqrt{3}\,a^2} = \frac{2}{\sqrt{3}}\left(\frac{N_A}{\sqrt{2}}\frac{\rho_s}{\mu}\right)^{2/3} \qquad \text{A-9}$$

Substitution of A-9 into A-7 yields the equation

$$\sigma = \frac{L_s\,\mu}{4\,N_A}\frac{2}{\sqrt{2}}\left(\frac{\rho_s}{\mu}\right)^{2/3} = .229\,\frac{L_s\,\mu}{N_A}\left(\frac{N_A\,\rho_s}{\mu}\right)^{2/3} \qquad \text{A-10}$$

Comparison of equation A-10 and A-1 shows that the constant .229 in A-10 is approximately 15-percent lower than the constant in A-1. Therefore, equation A-10 would predict a lower surface energy than Tabor's expression.

TABLE 1.- BEATTIE-BRIDGEMAN EQUATION OF STATE CONSTANTS FOR NITROGEN, REF. 6

A_o = 173.60 N-m^4/kg^2

a = .0009342 m^3/kg

B_o = .001801 m^3/kg

b = - .000247 m^3/kg

C = 1499. m^3k^3/kg

TABLE 2.- THERMAL CONDUCTIVITY FOR NITROGEN, $\frac{J}{m\text{-}K\text{-}sec}$,
JACOBSEN REF. 24

$$\lambda = \lambda_0(T) + \Delta \lambda_E(\rho)$$

$$\lambda_o = \sum_{i=1}^{a} A_i \, T^{(i-3)}$$

$$\Delta\lambda_E = .00002195902219\ \rho + .006387370699\ (e^{.0036\ \rho} - 1.0)$$

$$A_1 = -6.8939127475$$

$$A_2 = 3.5226118983 \times 10^{-1}$$

$$A_3 = -6.8357539823 \times 10^{-3}$$

$$A_4 = 1.5832717315 \times 10^{-4}$$

$$A_5 = -2.6418423047 \times 10^{-7}$$

$$A_6 = 3.6093309138 \times 10^{-10}$$

$$A_7 = -2.5555598476 \times 10^{-13}$$

$$A_8 = 8.5635041641 \times 10^{-17}$$

$$A_9 = -1.0717599406 \times 10^{-20}$$

TABLE 3.- VISCOSITY FOR NITROGEN, $\frac{\text{N-sec}}{\text{m}^2}$,

JACOBSEN REF. 24

$$\eta = \eta_o(T) + \Delta\eta_E(\rho)$$

$$\eta_o = \sum_{i=1}^{9} C_i T^{(i-3)}$$

$C_1 = 7.4165322904 \times 10^{-3}$

$C_2 = -1.5834400475 \times 10^{-4}$

$C_3 = 3.8530771011 \times 10^{-7}$

$C_4 = 8.0133713668 \times 10^{-8}$

$C_5 = -8.9203123846 \times 10^{-11}$

$C_6 = 8.9059711315 \times 10^{-14}$

$C_7 = -5.3779372664 \times 10^{-17}$

$C_8 = 1.7398277309 \times 10^{-20}$

$C_9 = -2.3084044942 \times 10^{-24}$

$$\Delta\eta_E = \sum_{i=1}^{7} D_i (0.001\rho)^i$$

$D_1 = 2.3083514362 \times 10^{-5}$

$D_2 = -9.3636207171 \times 10^{-5}$

$D_3 = 9.0339186452 \times 10^{-4}$

$D_4 = -4.1832067163 \times 10^{-3}$

$D_5 = 1.0897627893 \times 10^{-2}$

$D_6 = -1.2913856376 \times 10^{-2}$

$D_7 = 5.9782049913 \times 10^{-3}$

TABLE 4.- VAPOR PRESSURE CURVE

$$p_{sat} = c \bullet 10^{(a-b/T)}$$

Reference	Dodge and Davis Ref. 29	Frels, et. al. Ref. 30
Range	63.148<T<126.20 K	35.5<T<63.148 K
a	3.93352	7.614676
b	304.494 sec	356.281 sec
c	101325 N/m^2	133.32 N/m^2

TABLE 5.- COMPARISON OF PREDICTED CONDENSATION ONSET TOTAL TEMPERATURE

CAST-10 AIRFOIL. $M_\infty = 0.65$, $p_t = 5.0$ atm

BASELINE-CLDT, $T_t = 99K$, $\Delta C_p = 0.0266$, $x/c = 0.25$

Modification	Onset T_t, K	T_t - 99K	J/J_{CL}
CLDT	99	0	1
CLDT-T, $\delta = 0.25 \times 10^{-10}$m	100.7	1.7	500
CLDT-RK	100.3	1.3	110
CLDT-LP, $Q_{rep} = 10^8$	103.8	4.8	10^{11}
Nonisothermal	98	-1.0	.046
CLDT, σ reduced 10%	102	3	10^6
CLDT, B-B equation of state	99.8	.8	18

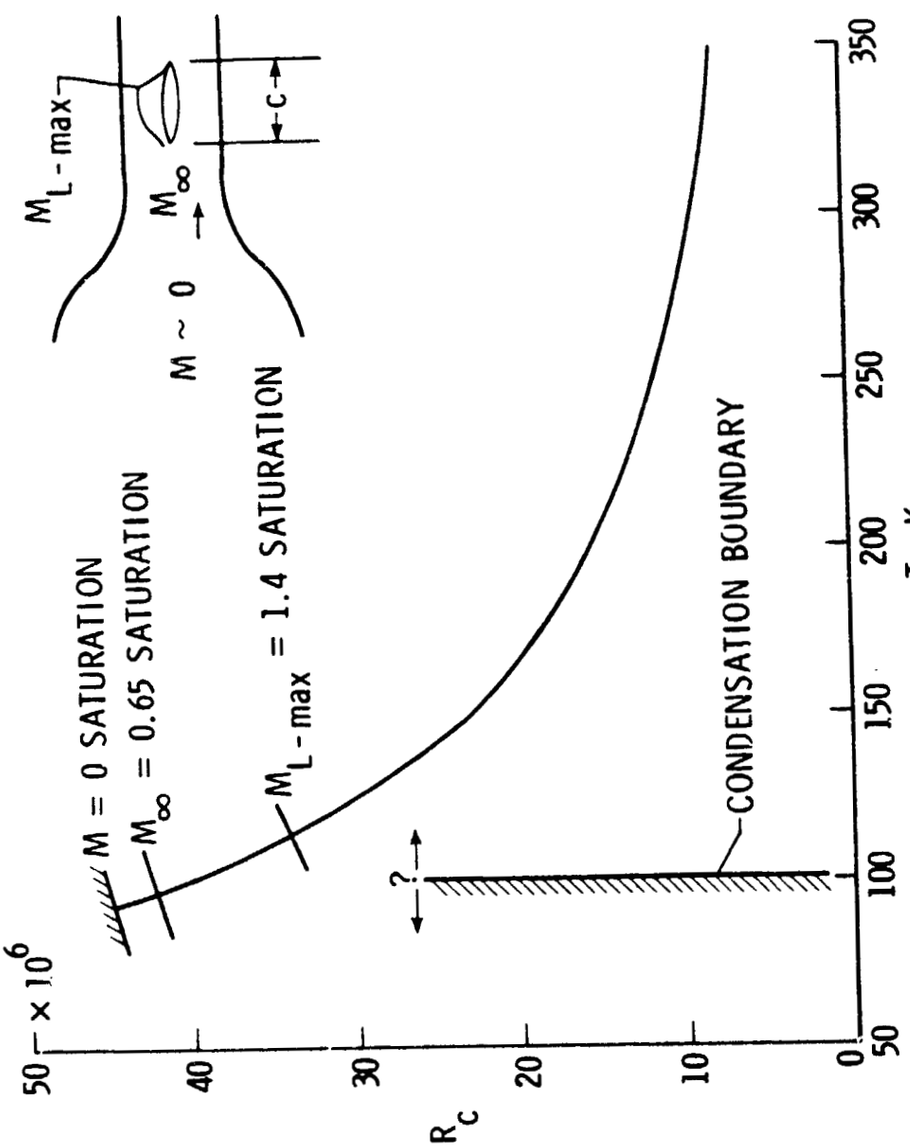

Figure 1.- Effect of reducing total temperature on Reynolds number. M_∞ = 0.65, p_t = 5 atm, c= 0.152m. Nitrogen gas.

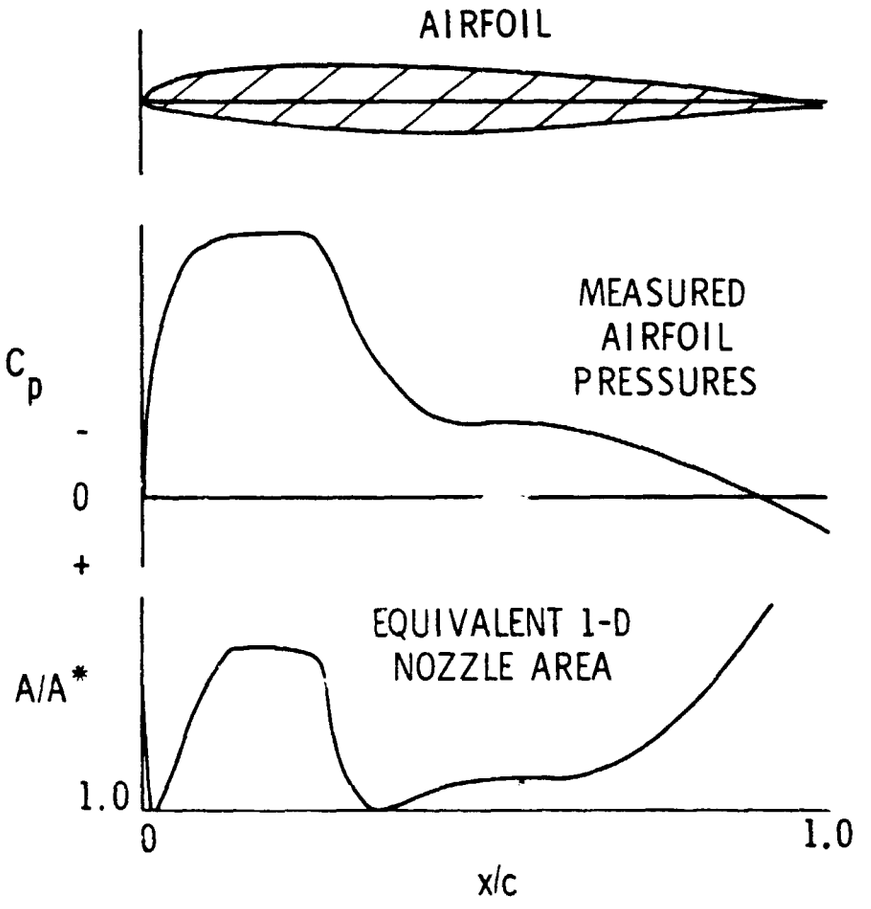

Figure 2.- Approximating airfoil pressure distribution by an equivalent one-dimensional nozzle.

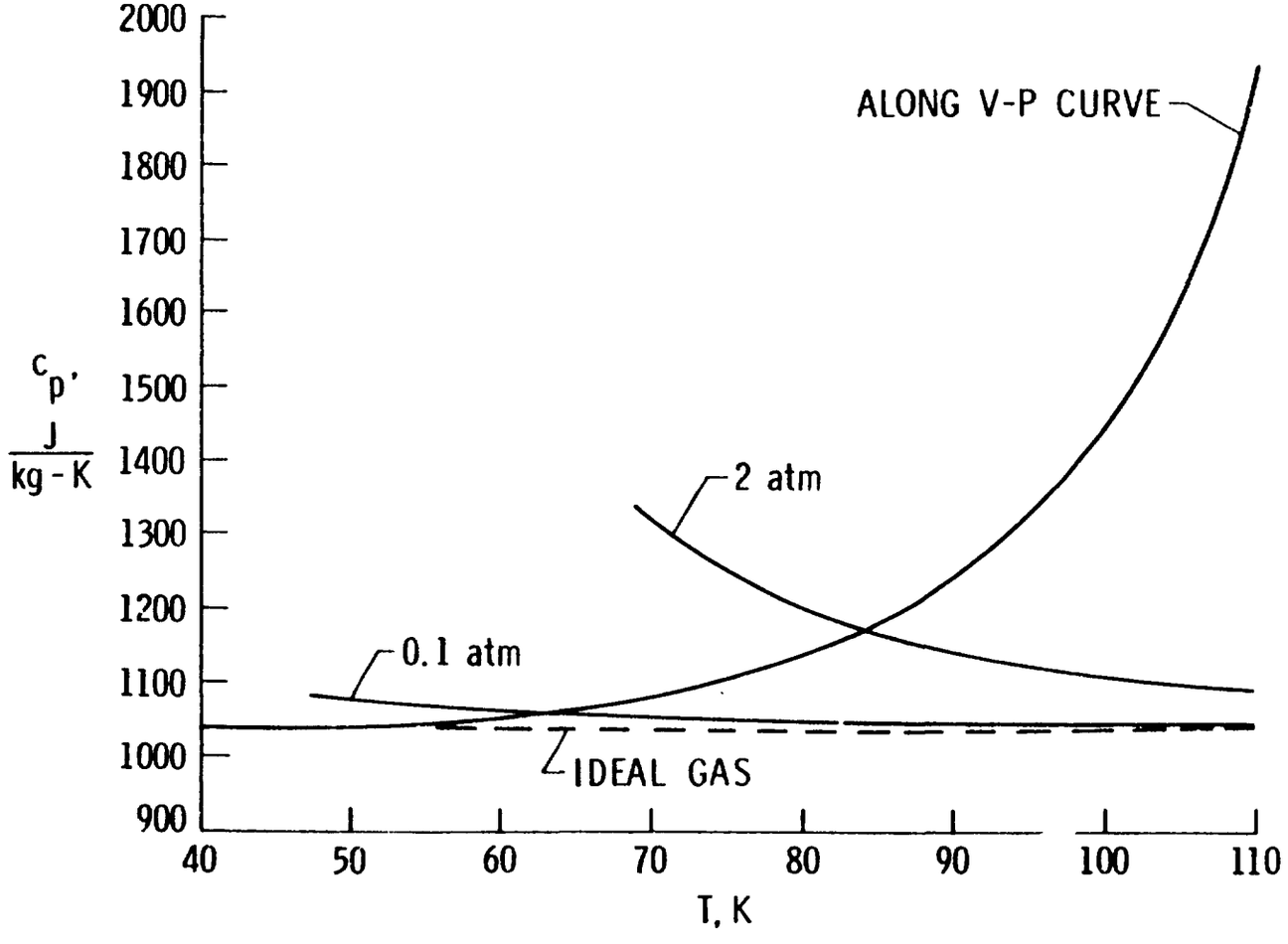

Figure 3.- Comparison of specific heat at constant pressure as a function of temperature plotted for constant pressures of 0.1 and 2 atm and for the pressures associated with the vapor-pressure curve using the Beattie-Bridgeman equation of state with the ideal gas value.

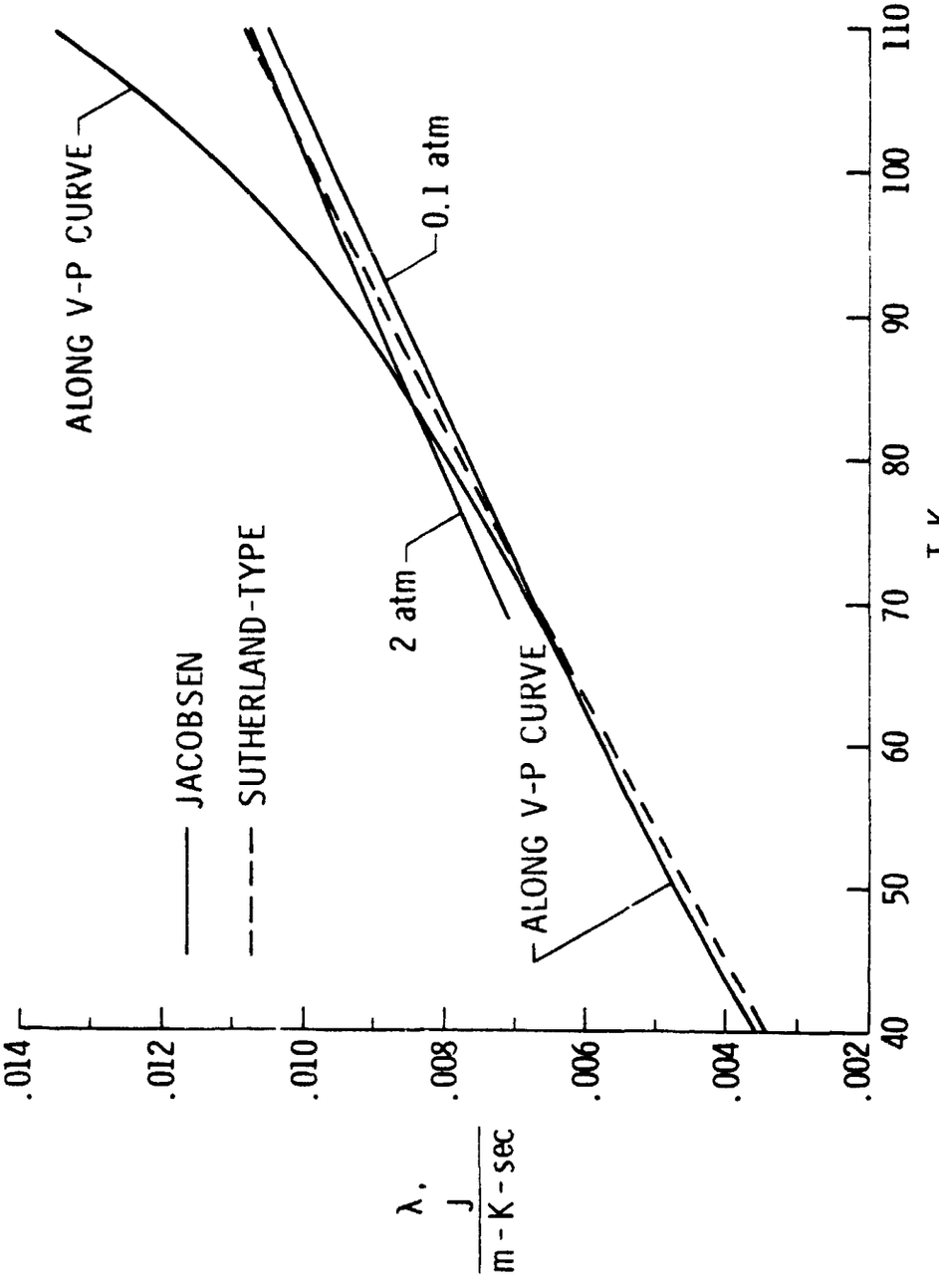

Figure 4.- Thermal conductivity of nitrogen gas.

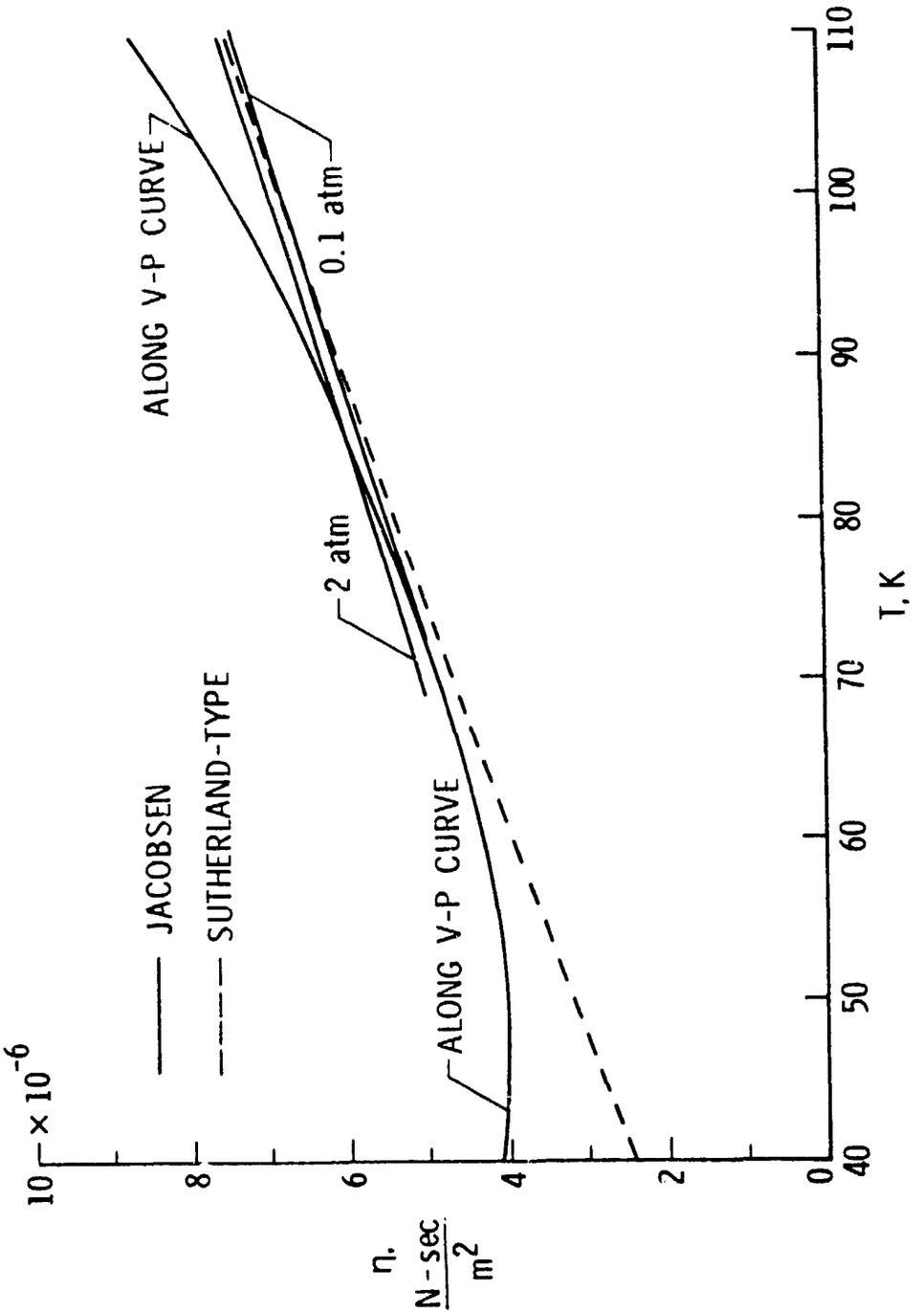

Figure 5.- Viscosity of nitrogen gas.

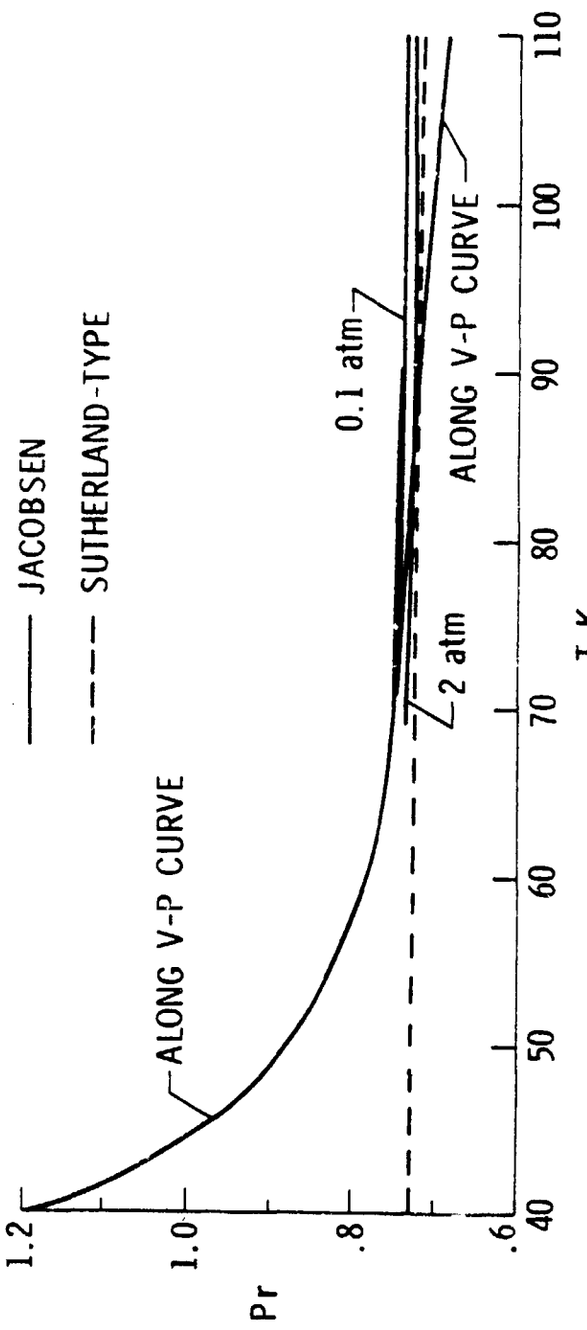

a) Both Jacobsen and Sutherland-type λ and η and ideal gas c_p.

Figure 6.- Prandtl number calculated using either Jacobsen or Sutherland-type λ and η combined with c_p from either Beattie-Bridgeman or ideal gas equation of state.

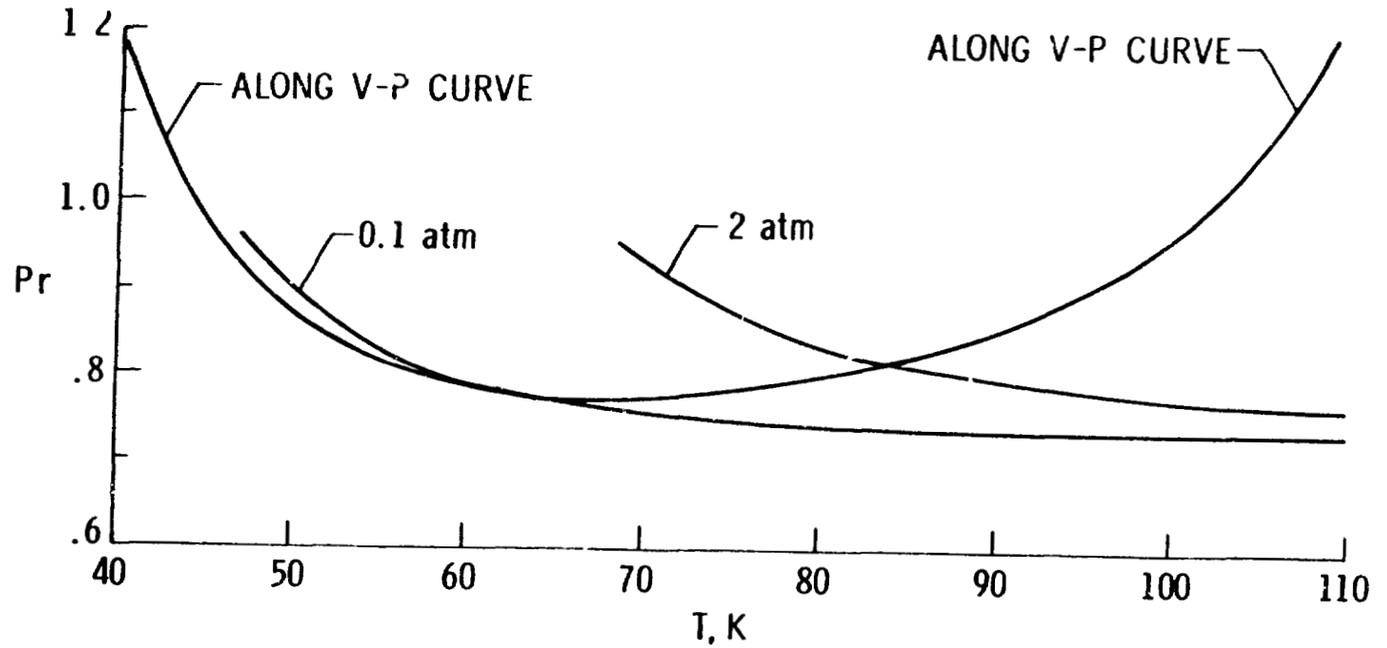

b) Jacobsen λ and η and Beattie-Bridgeman c_p.

Figure 6.- Continued.

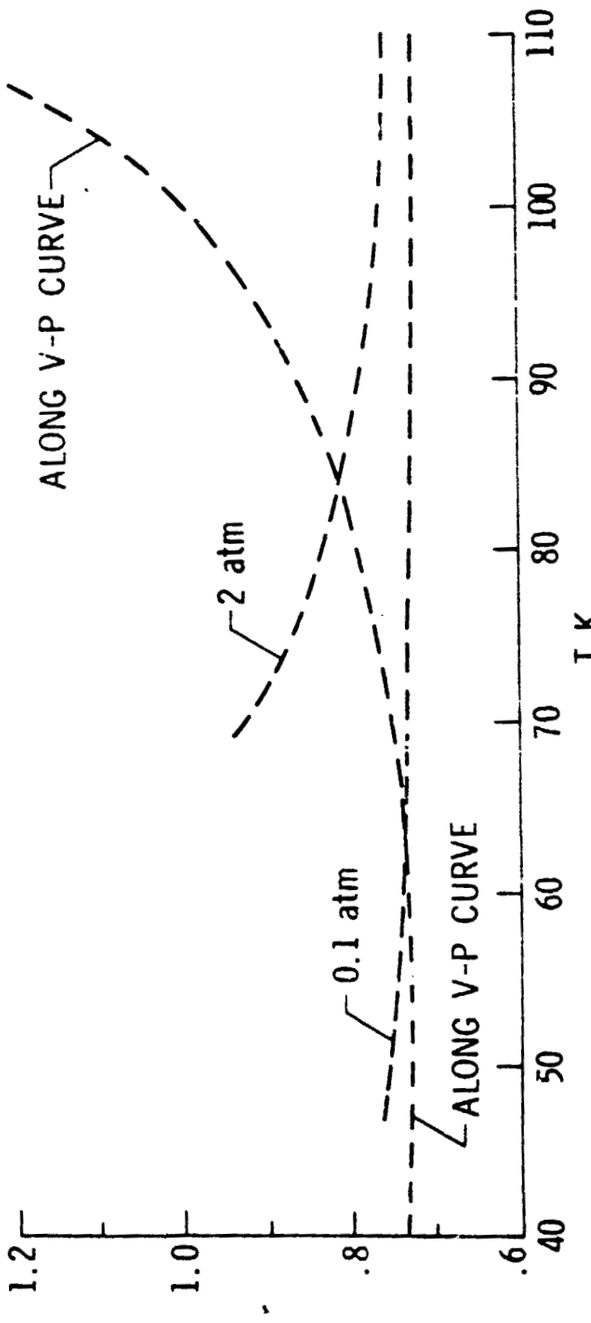

c) Sutherland-type λ and η and Beattie-Bridgeman c_p.

Figure 6.- Continued.

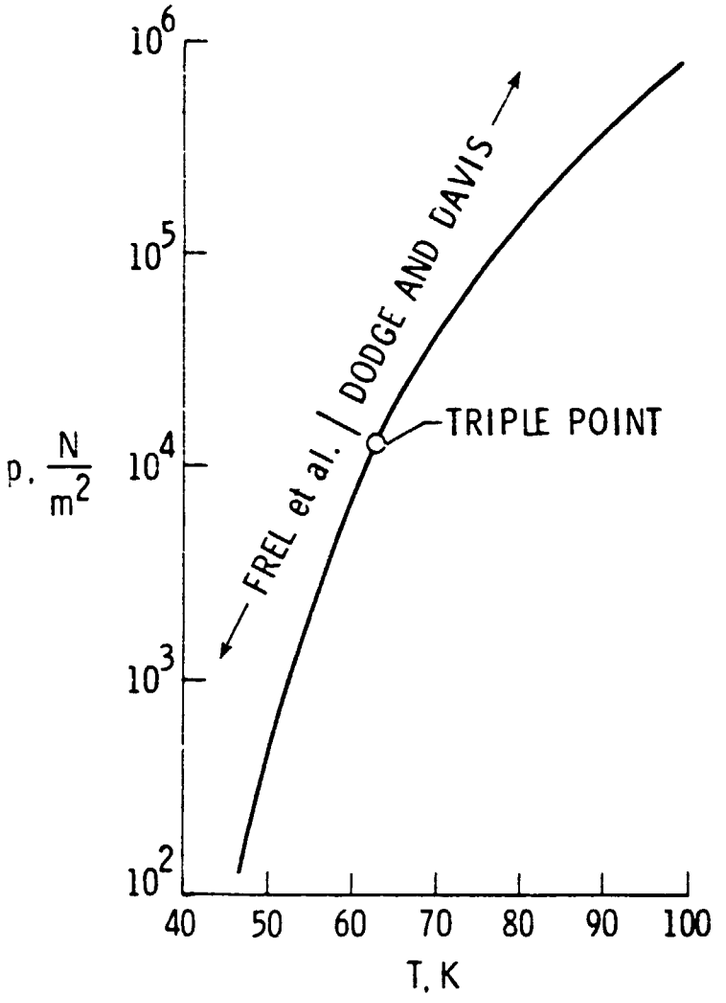

Figure 7.- Vapor-pressure curve for nitrogen.

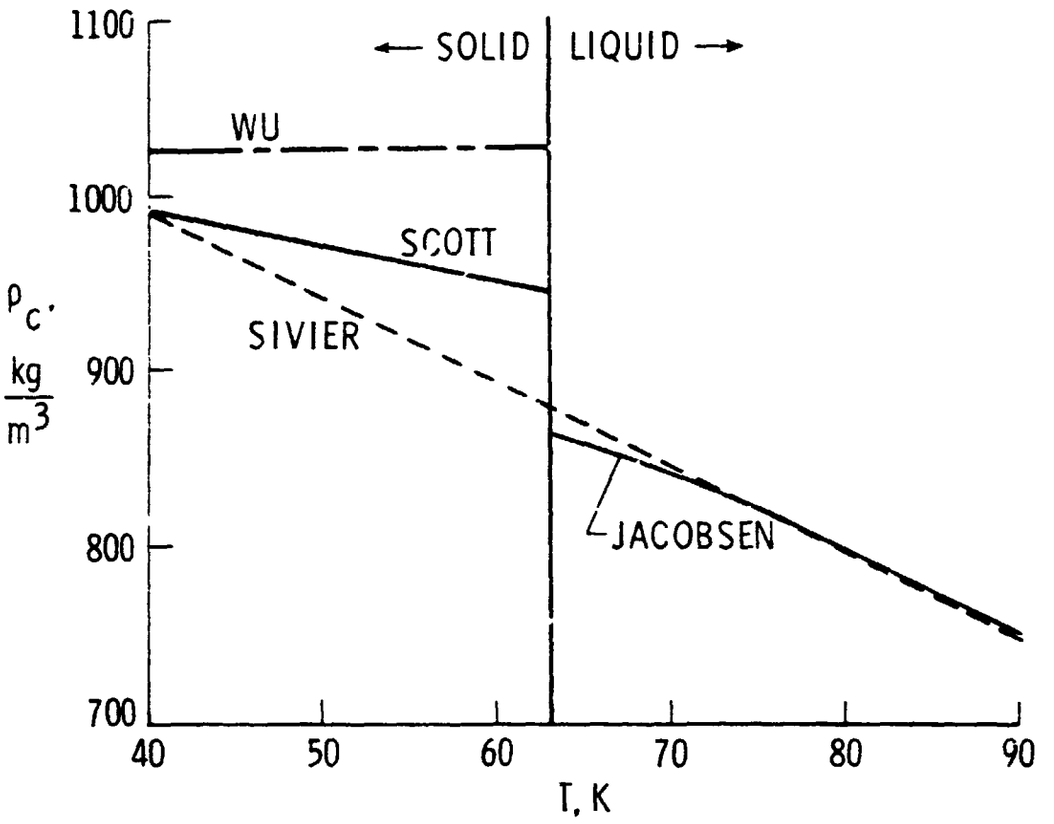

Figure 8.- Condensate density for nitrogen.

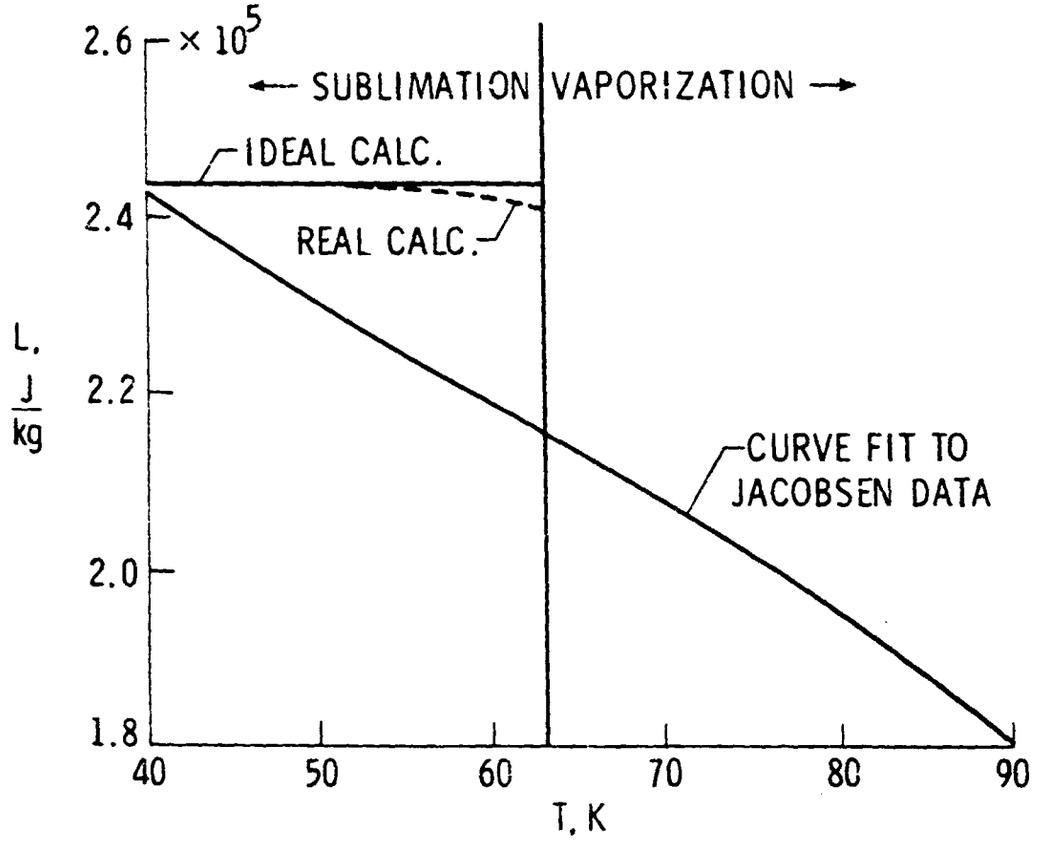

Figure 9.- Latent heat values for nitrogen. Line labeled IDEAL CALC. uses ideal gas equation of state values for gas density while line labelled REAL CALC. uses Beattie-Bridgeman equation of state values of gas density.

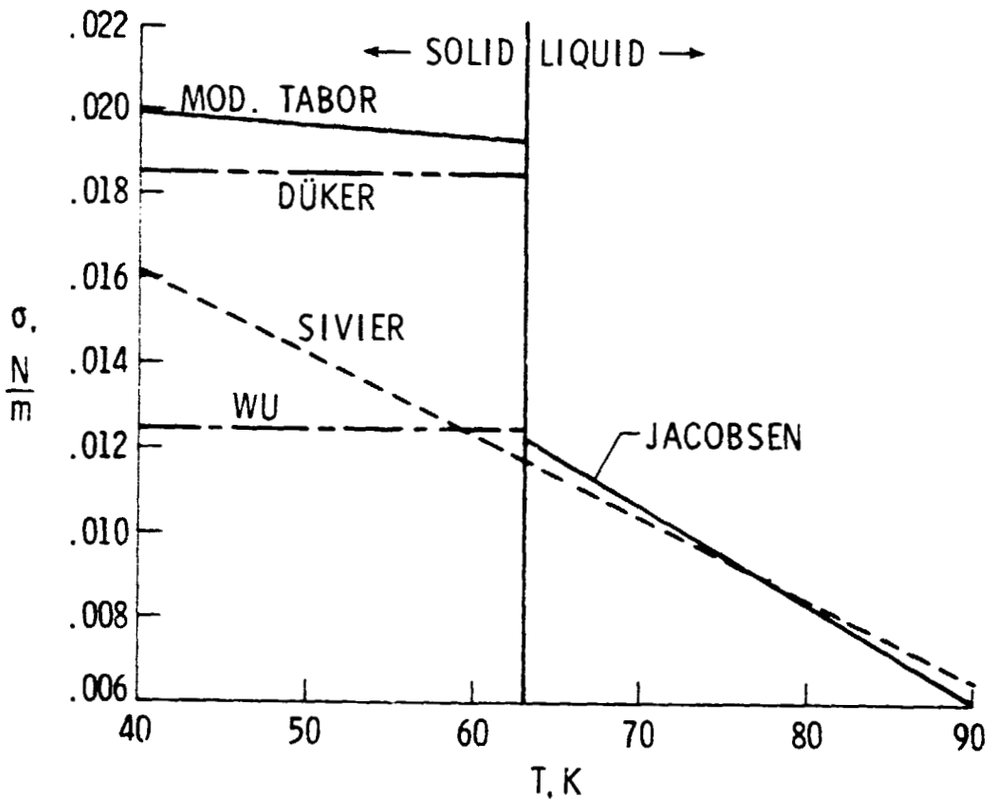

Figure 10.- Surface tension for nitrogen.

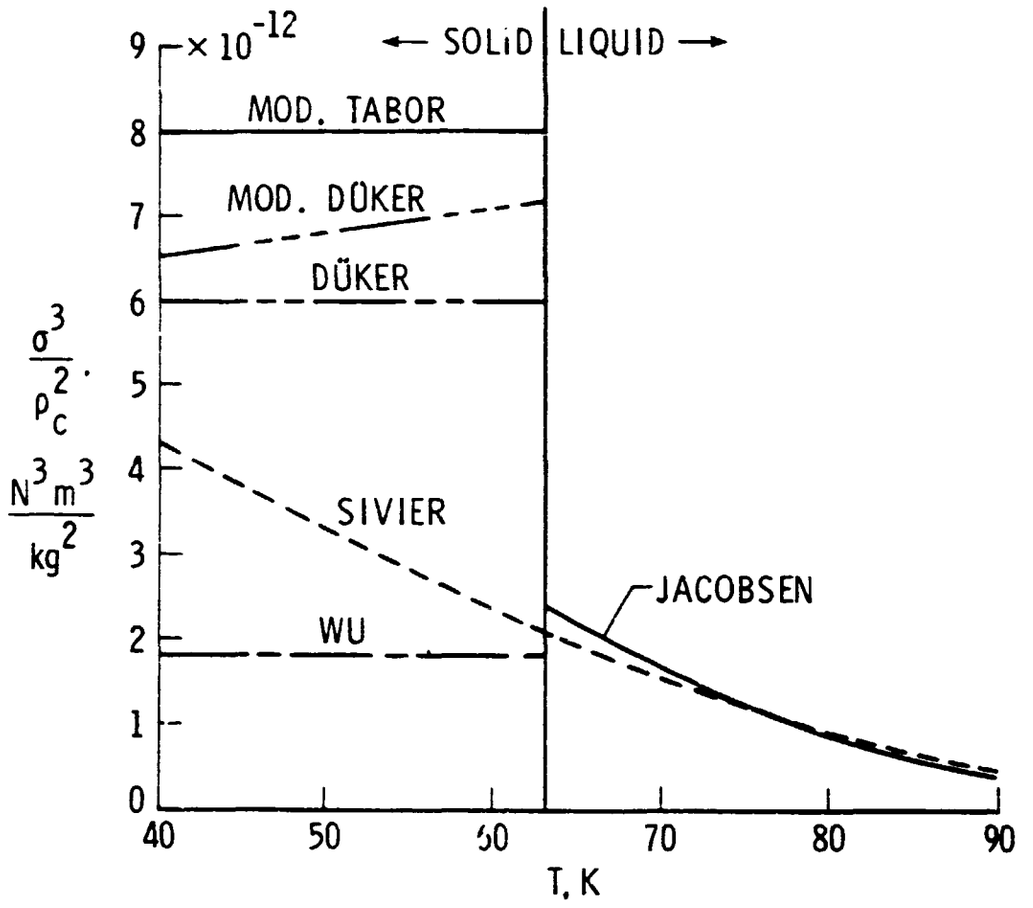

Figure 11.- Comparison of different expressions for σ^3/ρ_c^2.

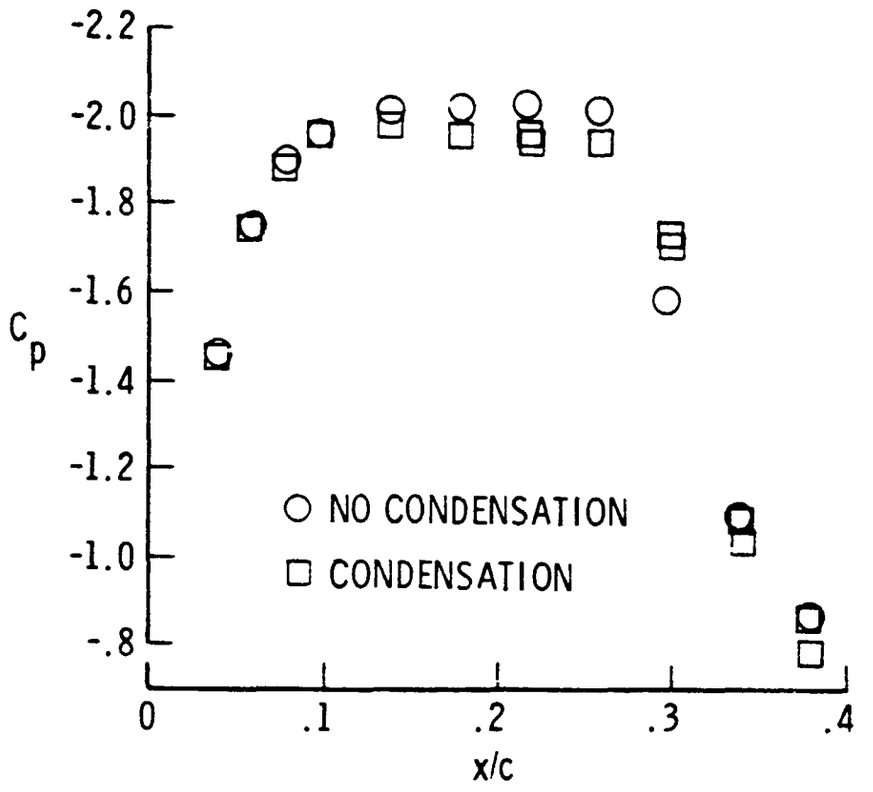

Figure 12.- Pressure coefficients in region of interest for CAST-10 airfoil. M_∞ = 0.65, α = 6^0, and c= 0.152m.

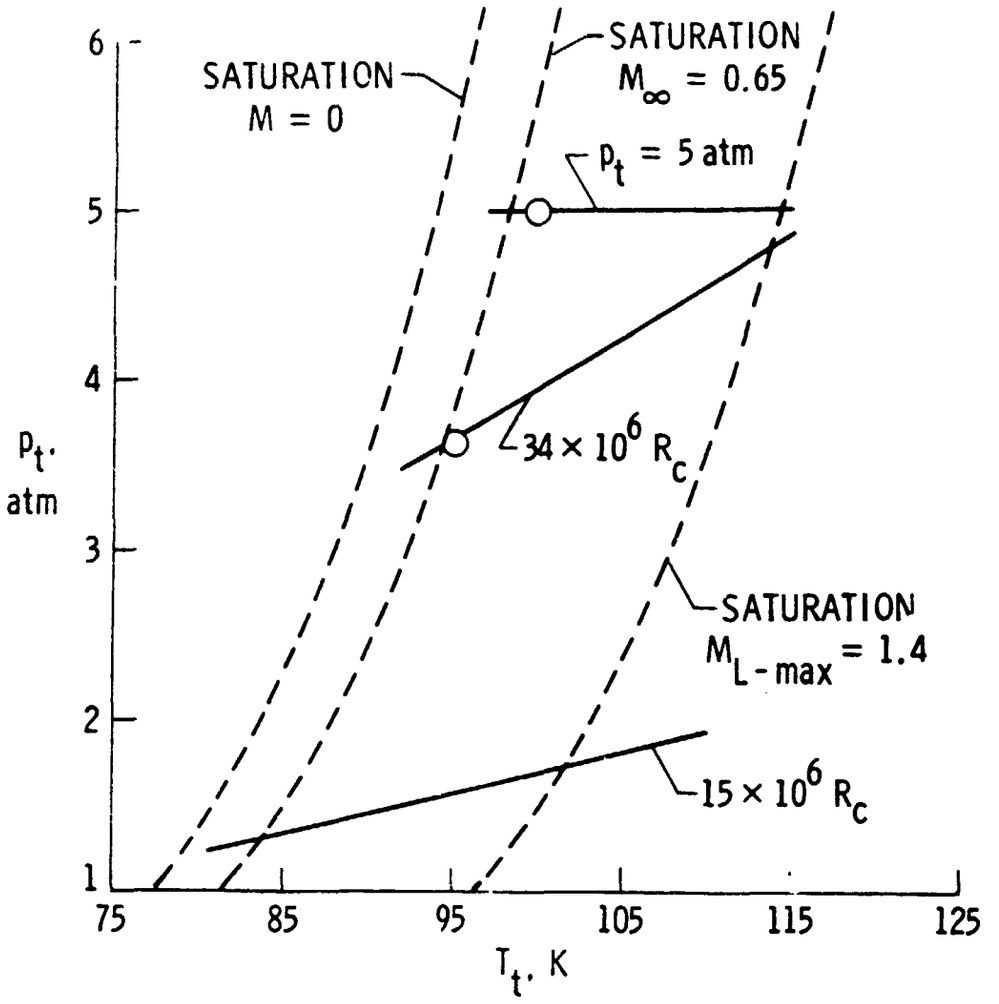

Figure 13.- Saturation lines as well as lines showing total conditions for CAST-10 airfoil at $\alpha=6^0$. O -Experimental onset of condensation effects.

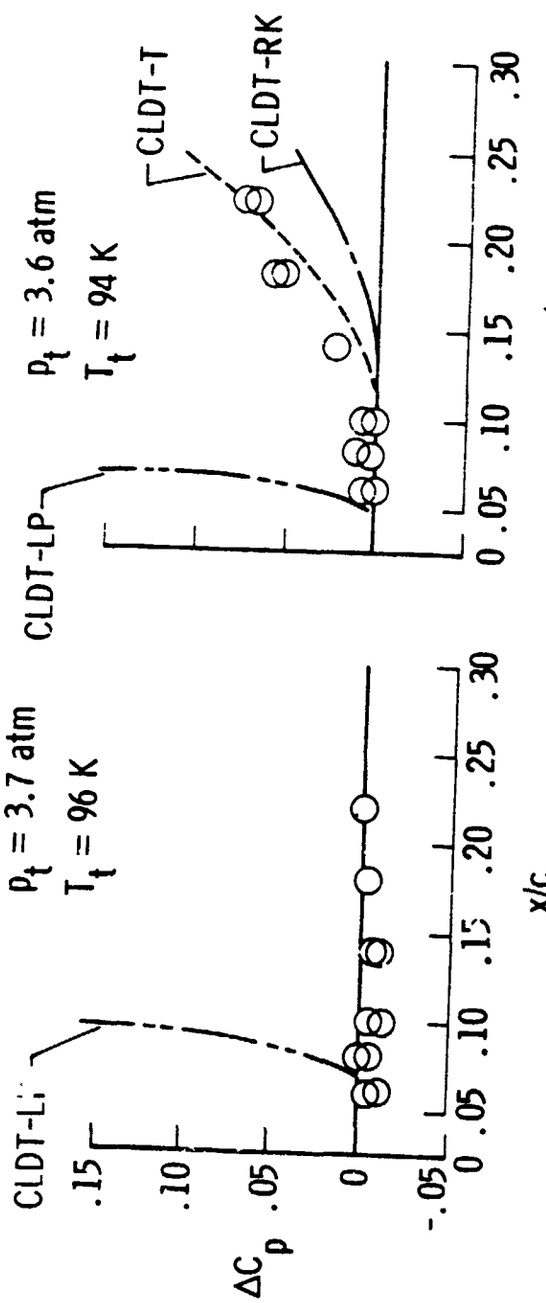

Figure 14.- Comparison of CAST-10 data, O, and theory for $R_c = 34 \times 10^6$, $M_\infty = 0.65$, $\alpha = 6^o$.

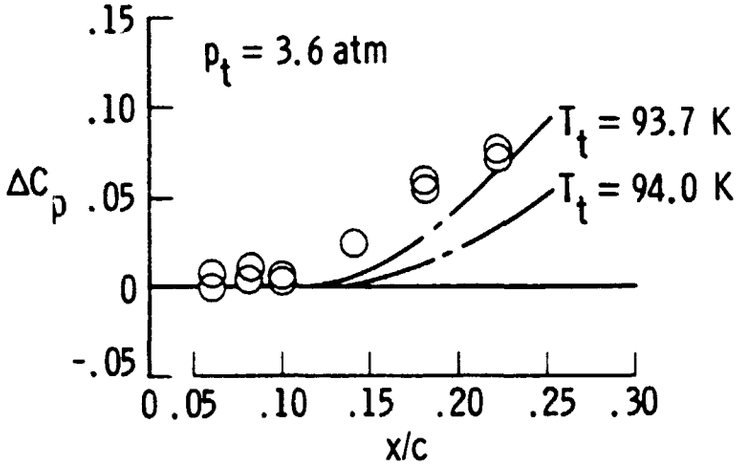

Figure 15.- Sensitivity of calculations to small T_t changes using CLDT-RK, —— – – –.

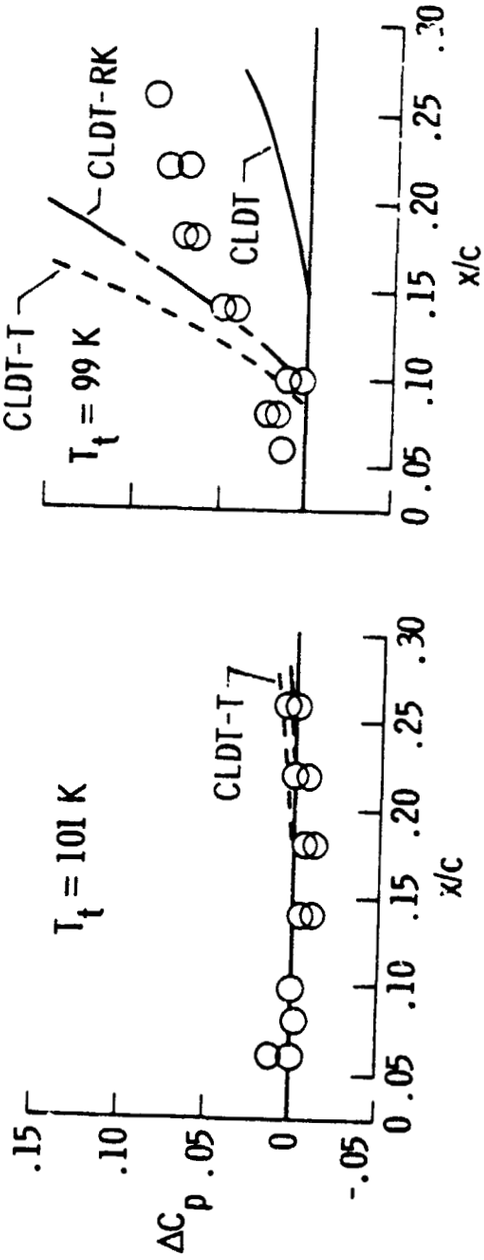

Figure 16.- Comparison of CAST-10 data, O, and theory for p_t = 5 atm, M_∞ = 0.65, α = 6°.

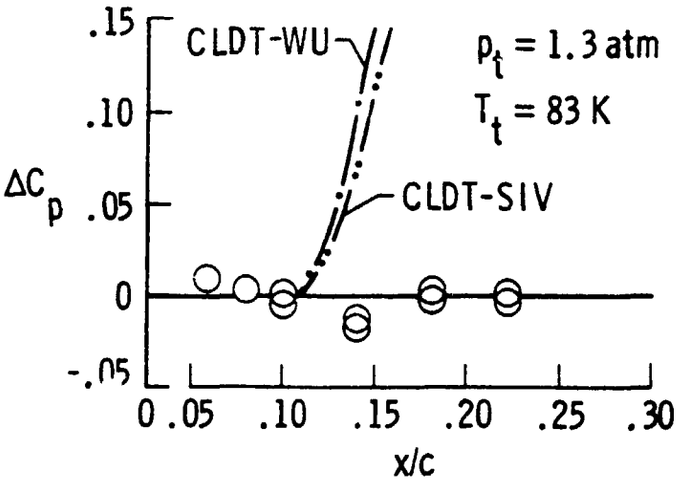

Figure 17.- Comparison of CAST-10 data, O, and theory for $R_c = 15 \times 10^6$, $M_\infty = 0.65$, and $\alpha = 6^o$.

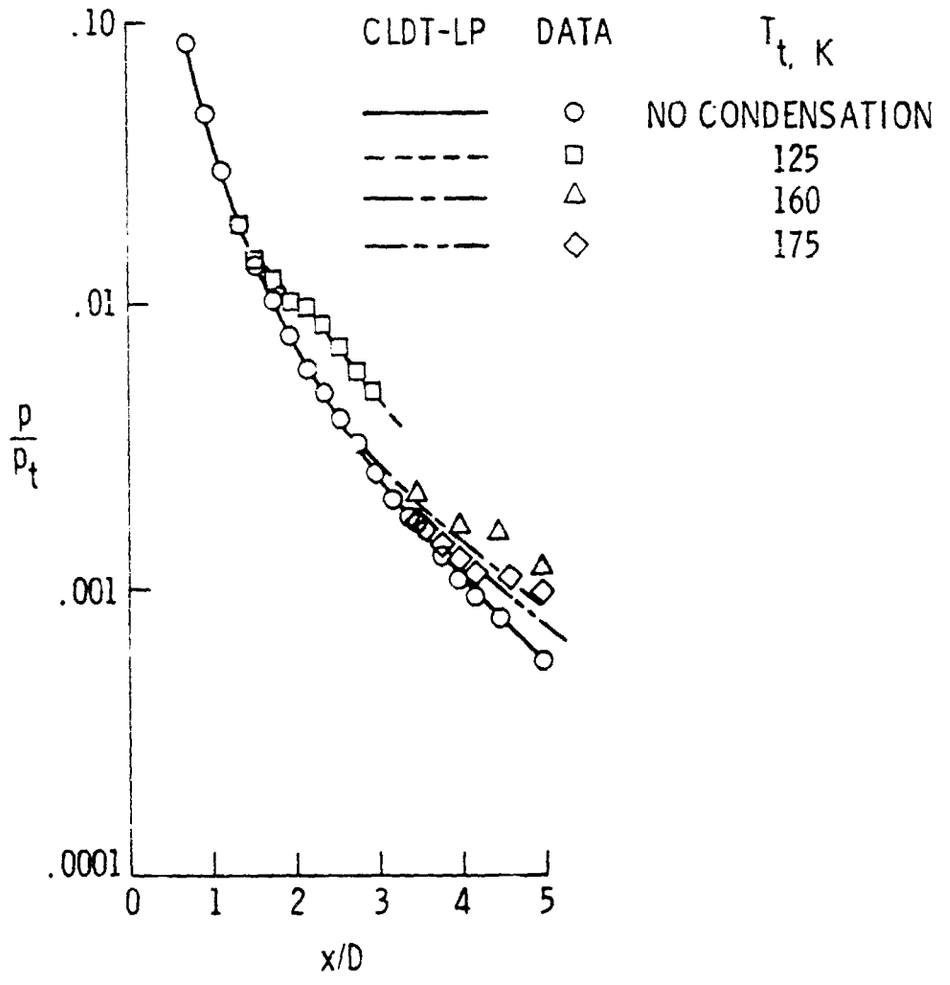

a) Comparison with CLDT-LP, $Q_{rep} = 10^4$.

Figure 18.- Comparison of Danket data and theory. Pressure ratio as a function of orifice diameters downstream of orifice. p_t= 3.0 atm, D= 0.005m.

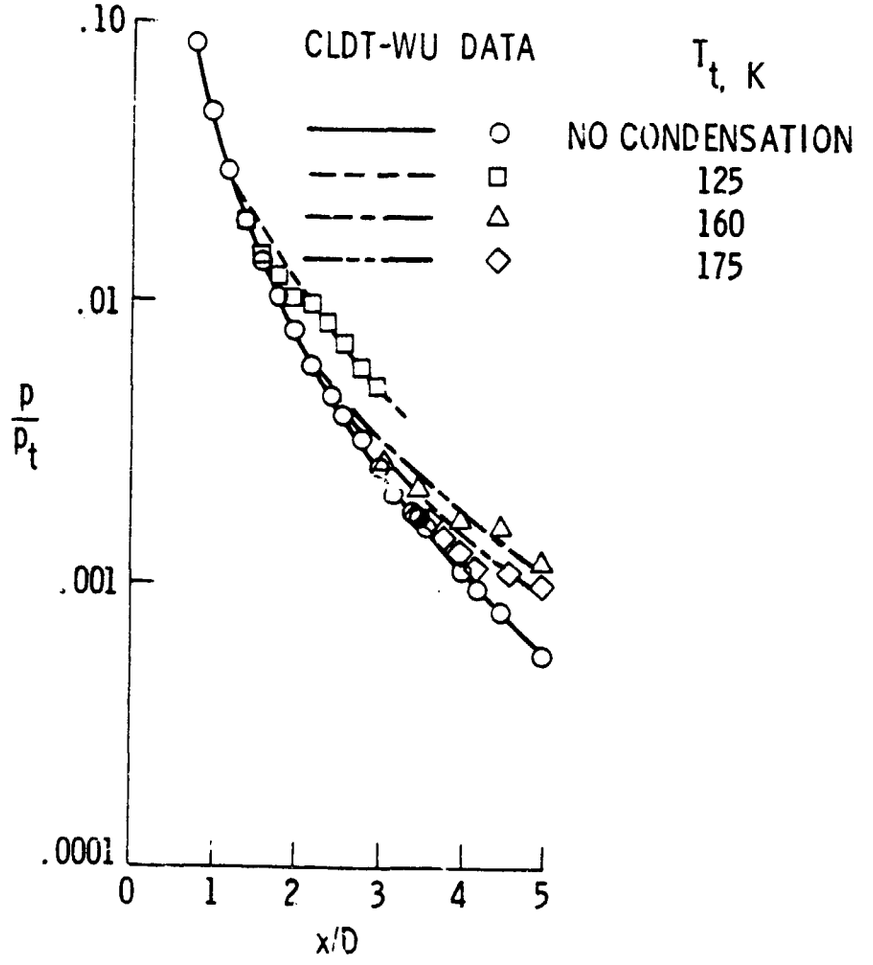

b) Comparison with CLDT-WU.

Figure 18.- Continued.

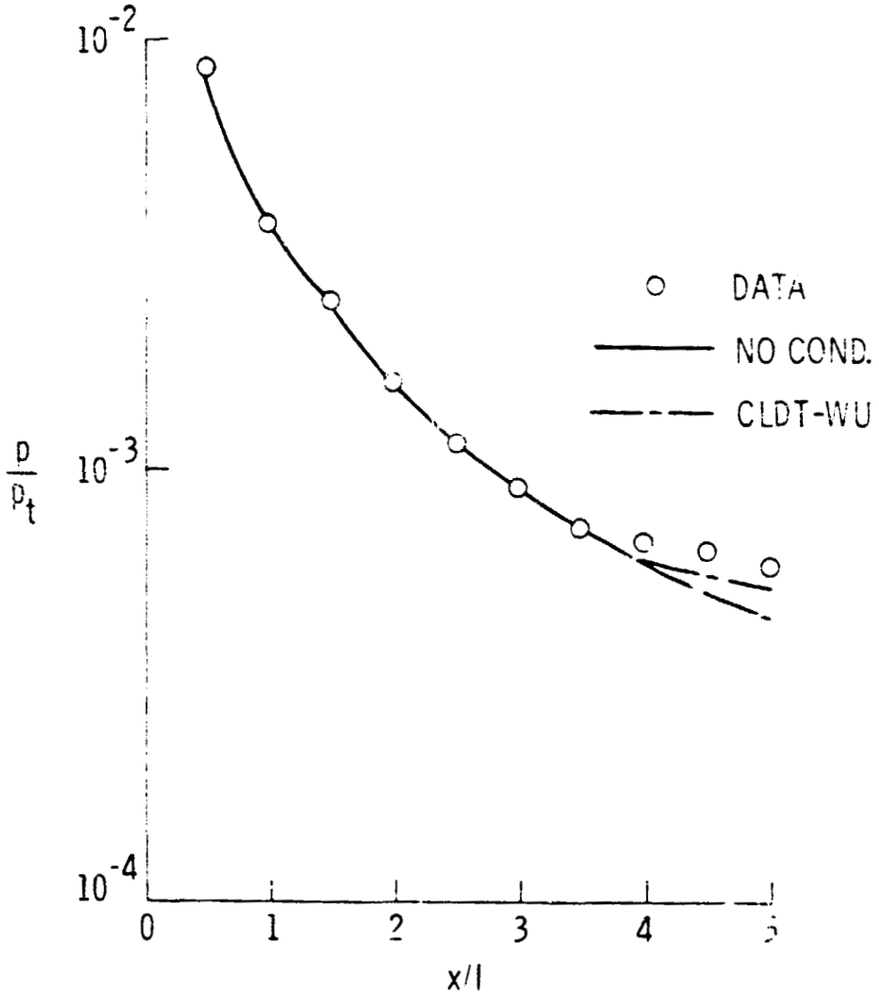

Figure 19.- Comparison of Nagamatsu and Willmarth data and CLDT-WU. Pressure ratio as a function of position. P_t= 8.21 atm, T_t= 295 K, and I= 0.0254m.

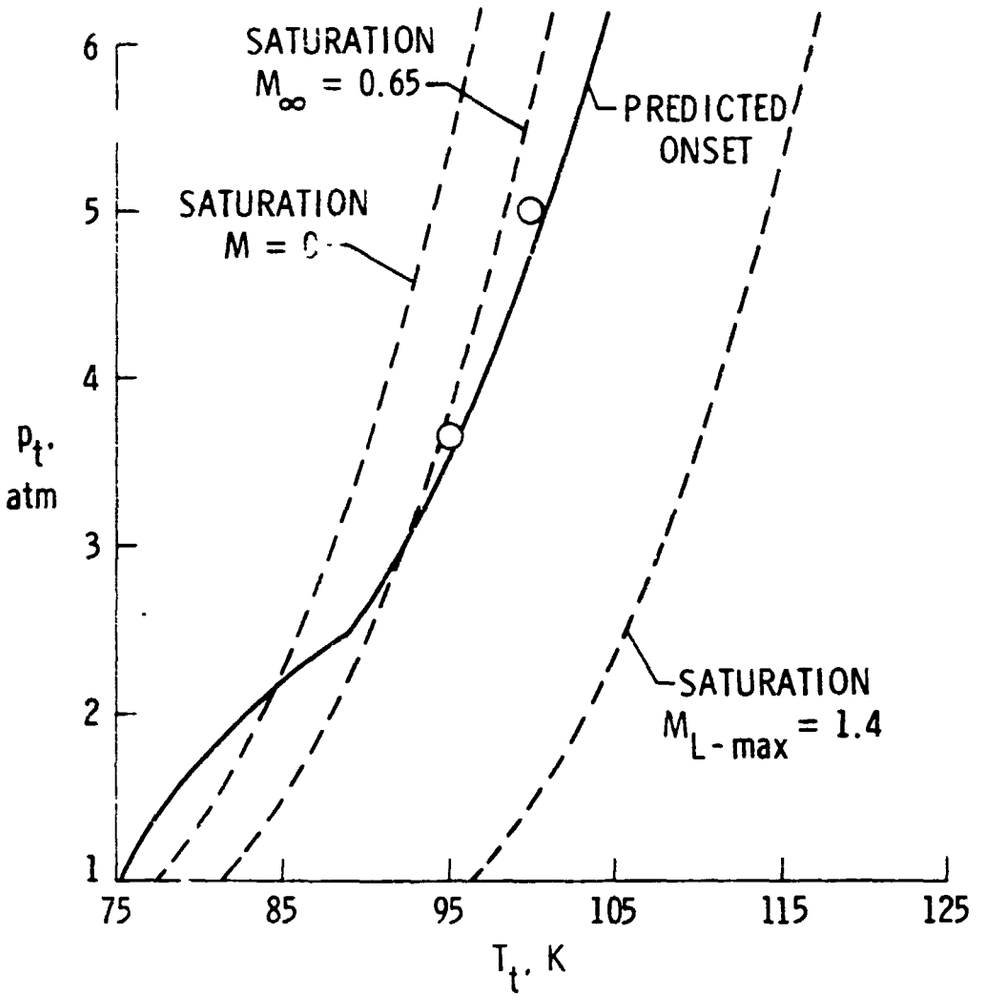

Figure 20.- Predicted onset curve for 0.152m CAST-10 airfoil. M_∞ = 0.65, and $\alpha = 6^o$. O -Experimental onset of condensation effects.